©Copyright 2014
Charles B. Matlack

Adaptation for Brain-Computer Interfaces

Charles B. Matlack

A dissertation
submitted in partial fulfillment of the
requirements for the degree of

Doctor of Philosophy

University of Washington

2014

Reading Committee:

Howard Jay Chizeck, Chair

Chet T. Moritz

Emanuel V. Todorov

Program Authorized to Offer Degree:
Electrical Engineering

University of Washington

Abstract

Adaptation for Brain-Computer Interfaces

Charles B. Matlack

Chair of the Supervisory Committee:
Professor Howard Jay Chizeck
Electrical Engineering

Brain-computer interface (BCI) technology is evolving rapidly, and shows promise for restoring and even augmenting dextrous control of movement. Recent studies have demonstrated control of robotic arms and computer cursors for basic positioning and manipulation tasks, using signals recorded from cortex. It is clear, however, that substantial improvements are required to achieve the level of reliability and dexterity to enable clinical translation.

BCIs present an instance of the dual control problem, wherein a controller is challenged with two distinct but inseparable problems: identifying a novel system, and concurrently driving that system to a desired state with minimum effort. This thesis addresses basic questions about how the brain adapts to novel movement control tasks. Based on models validated in human-computer interface (HCI) studies, we first develop a performance metric for comparing manual and brain control of positioning tasks. Next, we explore existing HCI study results on control gain selection for novel interfaces, yielding insights about gain selection consequences which are conserved across interface modalities. Finally, we identify a simple control policy structure which is evident during both brain and manual control. This yields the finding that the brain acts upon both delayed and predicted task state information in its control policies. Together, these findings enable more standardized investigation of BCI performance, and open new possibilities for performance improvement.

TABLE OF CONTENTS

Page

LIST OF FIGURES

GLOSSARY

BCI: Brain-Computer Interface.

CD GAIN: Control-Display gain, the scaling ratio between movement as displayed on a computer screen or other visual feedback mechanism, and user-generated command signals or physical motion.

ECOG: Electrocorticography, recording of electrical activity from inside the skull but outside the dura.

EEG: Electroencephalography, recording of electrical activity from the scalp without penetrating the skin.

ID: Index of Difficulty, the term in Fitts's law quantifying the inherent difficulty of a task, independent of the interface or subject.

TASK GEOMETRY: Comprises a specific distance and target width in an aimed reaching or cursor control experiment; not to be conflated with a specific ID, which encompasses the set of tasks geometrically similar under re-scaling.

ACKNOWLEDGMENTS

I'd first like to thank Robert Robinson for his expert monkey wrangling and sense of humor. He saved me untold frustration and provided valuable input on experiment design. I'd also like to thank Professor Paul Sampson and Chad Young in the UW Statistics Department for invaluable advice on statistical analyses and, in particular, on the use of the log transformation in my performance metric work. I would especially like to thank Géry Casiez for providing me his data from human-computer interface studies he conducted 5 years ago, with permission to incorporate them in my own publications.

Howard Chizeck has supported and mentored me, both in my graduate research efforts and in other endeavors, with patience and a restrained style that allowed me to better understand how to manage myself. I cannot thank him enough for that. My de-facto co-advisor, Chet Moritz, has been tolerant of ideas outside of his comfort zone, allowed me the use of his experimental animals, and provided excellent and rigorous feedback on my writing and presentations, and on the writing process. Adrienne Fairhall and Emo Todorov have provided helpful feedback on my ideas from their domains of expertise. The UW Biorobotics lab, the Moritz lab, and other students working on neural engineering research, such as Jeremiah Wander and Dev Sarma, have also provided helpful feedback and conversations on ideas, experiment designs, and presentations. My friend and business partner Tyler Davis took up the slack when I focused my energy on finishing my Ph.D. I've also had the moral support of close friends, including Melanie Coerver and Chris Hammersley.

Finally, I'd like to thank my family for their patient support throughout this process: Margaret, Bruce, Katie, and my extended cousins.

DEDICATION

To my parents, Bruce and Margaret, who must have done something right.

Chapter 1

INTRODUCTION

Brain-computer interface (BCI) technology is evolving rapidly, and shows promise for restoring and even augmenting dextrous control of movement. Recent studies have demonstrated control of biomimetic robotic arms for basic positioning and manipulation tasks, using signals recorded from cortex. Others have achieved control of computer cursors by non-human primates with speeds approaching that of manual control. It is clear, however, that substantial improvements in all aspects of the technology are required to achieve the level of reliability and dexterity to enable clinical translation. The work represented in this thesis takes a step back from aggressive forward engineering efforts focused on marginal performance improvements, and instead seeks better foundational understanding of how the brain approaches movement control in novel contexts.

The contributions of this work are as follows: first, we choose among a few existing models of speed/accuracy tradeoffs in reaching movements, adapting one for the unique challenges of BCI contexts. Next, we build upon some recent work done with that model, which had identified a correlation between one model parameter and the scaling factor between user input and displayed output. In this investigation, we identify a framework for choosing the scaling factor to minimize movement times across an experimenter-chosen set of tasks. Finally, we use a very basic model architecture to identify the control policies employed by our subject during both manual control and BCI-mediated control of a cursor task. In particular, we establish that control is based on delayed and predicted task state, not just immediate task state. We provide more detail on each of these contributions below.

1.1 Motivation and Significance

Quantitative performance metrics are a valuable basic tool for comparing different BCI designs and usage paradigms. Alternatives, such as functional assessments based on task completion, e.g. those used to measure stroke rehabilitation, are difficult to interpret and may not reveal subtle marginal differences.

Several models which predict (e.g. reaching) movement time as a function of distance and target width have been introduced, beginning with Fitts's law [22] in 1954 and including Welford's Model [67]. A review of the evolution of these models reveals an interesting story.

Fitts's law, in the formulation introduced by I.S. MacKenzie [40], equates one of the model parameters with information transfer rate in *bits/sec*. While this gives it tremendous appeal as a single, meaningful, quantitative performance measure, the unfortunate reality is that this assertion was never grounded in mathematics. Further, the model has poor descriptive power compared to the slightly more complex Welford's model. For additional details, we review the literature on this topic in 2.3.

We find that movements which must be terminated by *dwelling* over the target have a log-normal distribution of times, allowing us to adapt Welford's model to describe movement times in both BCI and manual tasks. This represents a more rigorous and standardized approach than using Fitts's law: it leaves behind the unrealistic hope of meaningful yet abstract descriptive power in Fitts's law, in favor of a model providing specific time predictions for specific task geometries.

Our selection and adaptation of a movement model as a performance metric leads naturally into an investigation of how the scaling factor, or gain, between user input and displayed task output affects performance. Decades of engineering optimizations to computer mice and pointing devices have resulted in speed-dependent gains, or acceleration profiles, a paradigm to which academic studies have not yet caught up [7].

Between this state of the art, and the lack of a gain adjustment in the human arm, investigating the effects of control-to-display gain may seem an 'academic' pursuit. However, the question of adjusting gain becomes very relevant for novel interfaces, especially those meant to provide control over task geometries outside the scale of normal human movements.

For example, [54] investigates the use of a Wii Remote, or more generally hand gestures, as a pointing interface for large displays. Brain-computer interface control provides a similar challenge: how do we pick the gain to maximize performance, and what about ease of use?

By investigating the effect of gain on the surface representing our model's predictions of movement time as a function of target distance and width, we gained novel insights. First, we establish the fact that asking a user to make the exact same movement, but with scaled-down visual feedback of the task, incurs a movement time penalty (increase). This is consistent with studies of force-tracking, such as simulated braking of a car.

Next, we show that when our model parameter of interest, k, is closest to 1, the time prediction surface is the most flat. This means that movement times have the least variation across different task geometries. Compared to gain choices which minimize movement times for a narrow set of task geometries, this gain outperforms other choices when the range of evaluated task geometries is expanded. This is important, because it means that trial-and-error gain optimization for minimum movement time is biased by the set of tested tasks, and that the resultant gain may not perform well outside that set of tasks. Fortunately, the model lets us predict when this will happen by extrapolating the fitted surface. This concept is best understood with illustrations, which are provided in Chapter 3.

Concluding our investigation of gain, we compare performance to reported ease-of-use. This question is informed by previous studies showing that subjects will increase effort when task difficulty is increased, suggesting that choosing a performance-maximizing gain is likely to conflict with effort minimization. Combining results of three different studies, we find that lower values of the k parameter (and gain) result in greater ease-of-use, with the smallest values tested only marginally less than 1.

In Chapter 4 we use tools from control systems and digital signal processing to guide an investigation in Chapter 5 of what control policies are used by the brain for movement control. We make two recommendations of best practices for system identification in neural control contexts. First, filtering input and output signals of the system under identification, using the same filter, imposes the experimenter's assumptions of system bandwidth on the recorded data. For example, under the rate-coding assumption, we should not attempt to correlate individual neuron spikes with arm movements. Filtering both input and output

also removes signal content which cannot be explained by the model, increasing R^2 values by effectively setting more reasonable expectations of model predictions. Gaussian filters, in particular, have been shown to work well for performing rate estimation from neural spike trains [53]. Our second recommendation is to use parsimonious models with a minimum number of parameters, which we show can be done without being constrained by the data sampling rate.

In Chapter 5, we seek a basic understanding of how the brain approaches BCI-mediated position control, and test the hypothesis that this strategy is similar to that used during a novel manual task. Gaining this understanding is important, because it will drive design decisions for BCI decoders that map neural activity to movement commands. BCIs present an instance of the *dual control* problem, wherein a controller is challenged to identify a novel system while concurrently driving that system to a desired state with minimum effort. Dual control problems do not admit separate optimal designs of a controller and estimator.

We show that a proportional-derivative controller is used, as well as control proportional to delayed and predicted task state. Our model has excellent explanatory power during manual control, and provides significant explanatory power of neural modulation during BCI-mediated control. That the controller model's descriptive power over manual effort decreases between manual and BCI control, whilst increasing over neural modulation, provides support for the hypothesis that neural modulation reflects an existing strategy applied to the novel interface. This contrasts with assertions that neural modulation for BCI control is achieved only indirectly, by continuing to execute the manual control policy [33].

An interesting detail of the control policy analysis is the result of estimating the delay and prediction intervals used. Although the confidence intervals are wide, we found no significant change in these intervals between manual and BCI control. This is surprising because the forward and feedback pathway latencies in the closed-loop task are changed dramatically by the switch to BCI control: the delays of neuromotor activation are eliminated, while feedback is restricted to the visual display, which is known to take much longer to process than proprioceptive or tactile input.

We conclude the thesis with a discussion of the knowledge gained by this work, the open

questions it has highlighted, and suggestions for further investigation.

1.2 A Word on Terminology

A topic of surprising divisiveness is whether neuroprosthetic technologies be referred to as brain-computer interfaces (BCIs) or brain-machine interfaces (BMIs). In this document we will refer to them as brain-computer interfaces (BCIs), as suggested by the title. In the submitted journal papers we will refer to brain-machine interfaces (BMIs) for consistency with the intracortical BCI community.

There are three perspectives we have considered regarding this matter: existing community standards, technical accuracy, and public perception. For reasons we have not tried to uncover and may not exist, the research community is split on this issue. The community of researchers focusing on non-invasive recording methods, as well as invasive methods which record from large areas of cortex such as ECoG, BCI is the dominant term. The community of researchers using microwire and microelectrode arrays to record from single units up to LFP (when the array recording quality degrades), BMI is the dominant term.

Regarding technical accuracy, we point out that information processing (computation), regardless of the physical substrate used to implement it, is a necessary component of a practical BCI. Computers are arguably a class of machine, but as machines all they do is turn electricity into heat; so too are neurons, using ATP to move small volumes of molecules back and forth over very short distances.

Finally, public perception: we believe this will become increasingly and critically important for steering nascent BCI technologies into acceptance first by patients and later by those seeking to augment normal function. Several examples of exist of scientific terminology choices selected and advocated for based on implied biases or assumptions of their connotations; perhaps the most famous is the championing of 'climate change' over 'global warming' by Frank Luntz and other conservative strategists. While the authors have their own feelings about *computer* vs. *machine*, the response of a lay audience to each term is much more important.

We think it is incumbent upon the scientific community, and practically speaking, the producers of the first BCIs for widespread use, to find out what terms create positive images

in the minds of a general audience, and to advocate terminology standards accordingly.

Chapter 2

BEYOND FITTS'S LAW: A STANDARDIZED AND ROBUST BCI PERFORMANCE METRIC

2.1 Chapter Summary

For brain-computer interfaces that provide the user continuous position control, there is little standardization of either performance metrics or evaluative tasks. Fitts's law, the model of human motor control recently applied to BCI tasks, lacks robust explanatory power [31] in its single "throughput" measure of performance [59]. A need exists for characterizing, in isolation, the quality of movement control afforded by a BCI. Movement control mediates, and is only indirectly measured by, symbol transmission via graphical interface. Consequently, characterizing differences between manual and BCI movement control is a fundamental prerequisite to optimizing complete system design for all uses, including discrete selection tasks.

Fitts's law is remarkably successful in describing aimed reaching movements across a wide range of interface modalities, recently including brain-computer interface (BCI) tasks [18, 55]. However, it is non-robust to large variations in task geometries [31]: while the model assumes that only the *ratio* of target distance to width (D/W) determines movement time, movements at identical ratios but different scale are observed to have significantly different times. While within-study comparisons of interface modalities have proven useful [41], the information transfer rate estimates derived from Fitts's law are inconsistent across studies [58]. This casts doubt on the utility of between-study comparisons based on throughput measures alone. Finally, Fitts's law is inconsistent with entropy: the index of difficulty term is *inspired by* information theory, but demonstrably inconsistent with it [59].

We provide a process for validating a movement model and identifying its parameters for data sets with many sub-optimal movement trials. This is done using a novel catch trial simulation method to confirm target-dependent feedback control by the user, then applying

a movement model to repeated measures data under a log-normal distribution assumption.

We use this process to show that the Shannon-Welford model [54] outperforms Fitts's law in describing movement times, after both are adapted for dwell-to-select tasks. These results, in combination with prior results using Fitts's law, suggest that movement models may be most valuable for making gross comparisons with manual control across a wide range of task parameters. Marginal comparisons within a single study are also possible, but their meaning depends critically on controlling parameters not explicity under investigation. Of particular concern in the BCI context is the practice of decoding intended velocity and integrating it to determine position during brain control, but not including an integrator in task dynamics during manual control. Finally, existing results in HCI studies suggest that movement models are not able to determine meaningful, marginal differences between studies [58]. Our results motivate and enable more extensive comparisons between native limb movement and even modestly-performing BCIs, which we believe are an important predictor of clinical utility.

The analyses shown here provide proscriptive information about BCI experiment design and enable fair performance comparisons between BCI and manual control of movement. We use a 1D cursor task controlled by cortical activity as a representative task for analysis. We then compare the ability of Fitts's law and of the Shannon-Welford model, both adapted for dwell-to-select tasks, to account for variability in movement trial times as a function of target distance and width.

From an ensemble of experimental data over many days, we identify the conditions under which the Shannon-Welford model outperforms Fitts's law.

Our results show that the Shannon-Welford model offers a better, and only marginally more complex, method of quantifying performance in both BCI- and manually-controlled positioning tasks. Although it does not provide a single aggregate measure, similar to the throughput measure estimated via Fitts's law, we show in Chapter 3 that one of the Shannon-Welford model parameters may provide deep insight into interface optimality. The model accurately predicts movement times, and motivates investigation, across a wide range of task geometries – a necessary validation of any BCI for clinical translation. The methods described here can address the shortcomings of existing performance metrics in the field,

and represent a significant step towards consistent methods of quantifying BCI performance and designing evaluative tasks.

2.2 Introduction

Standardized and straightforward metrics exist for quantifying symbol transmission rates, but not for characterizing the movement control mediating selection tasks. Performance metrics, including Fitts's law, are used in BCI studies to discern marginal performance differences between algorithm and experiment design variations. Their implementation, however, is not consistent, making comparison across studies difficult to impossible. For example, [55] uses the Shannon form of the index of difficulty, whereas [18] use the original form. Additionally, one assumes the model applies and directly calculates throughput based on a single task geometry [27], while others evaluate multiple geometries and report model parameters [18, 55]. As the state of the art of BCIs evolves, identifying the incremental contributions of individual design choices and making comparisons across studies will be critical for continued performance improvement.

The focus here is on maximizing information transfer rate, which has significant dependence on the graphical interface provided to the user. We believe that this approach is more relevant for the design of discrete selection interfaces, such as typing or menu navigation, and is less appropriate for evaluating open-ended movement control. By analogy, we expect words per minute to provide a more useful measure of keyboard design than of finger dexterity, and would not consider a cross-study comparison of dexterity possible without identical keyboards.

Our goal in this chapter is to develop methods to compare direct brain control of movement with manual limb movement. The extent to which a movement model accounts for trial times in a direct brain control task is as interesting and relevant as quantitative performance measures derived from model parameters. Trials with multiple task geometries are necessary to evaluate the predictive power of a model, which in turn is a prerequisite for its valid use as a performance metric. We evaluate the ability of Fitts's law and the Shannon-Welford model to describe trajectories observed in manual- and brain-controlled cursor positioning tasks performed by a macaque.

The rest of this chapter is organized as follows: in Section 2.3.2, we review the Fitts's law model and its prior use in analyzing BCI task performance; in Section 2.3.6 we introduce the Shannon-Welford empirical model and adapt it for BCI tasks; we next describe a simple 1D cursor control experiment in Section 2.4; in Section 2.5 we show which model best explains observed performance; and finally in Section 2.6 we address the implications of these findings.

2.3 Background

2.3.1 Performance Metrics in BCI Studies

Several approaches have been taken to quantifying the performance of BCI-mediated tasks prior to the introduction of Fitts's law.

One of the first and most persistent basic metrics is to report both trials per unit time and percentage of correct trials, with the latter being more relevant during early learning [4, 3, 43]. A drawback to this method is that it does not take into account task difficulty, nor can it accomodate mulitple task geometries or types into the same measurement. Marginally more information is provided by reporting moments of trial time histograms [46, 27], but this approach has the same drawbacks.

Properties of the trajectory taken to the target provide more nuanced insights into control qualtiy changes. These quantitative properties collectively considered to assess path efficiency include straightness, direction reversals, movement orthogonal to target vector, and path length [61]. An important problem with path efficiency is that it assumes an optimal trajectory without knowledge of the cost functions affecting the subject's control strategy. Even in the case of using a computer mouse, experimentally-observed trajectories are neither perfectly aimed, nor without overshoot and corrective actions near the endpoint [71].

A third popular method is to show average trajectories (after re-orienting many trajectories to match their directions), possibly highlighting the target-entry region [13, 27]. Trajectory information provides insight into differences between manual and BCI-mediated control, but averaging obscures corrective strategies near the endpoint. Also, the problem

of only evaluating a single task type and geometry exists here as well.

A few recent studies [55, 18, 27] use a model of aimed reaching movements adapted from the human-computer interface field. We discuss this in depth in the next section.

2.3.2 Fitts's Law and BCI Tasks

Some BCI studies of 1- or 2-D movement control derive information transfer rate (ITR) based on possible task outcomes [63, 52]. Other recent studies use Fitts's law to characterize performance and derive ITR [18, 55], or to estimate ITR directly under the assumption that the model applies [27]. For an excellent survey of recent BCI studies permitting ITR estimation via Fitts's law, see supplement to [27].

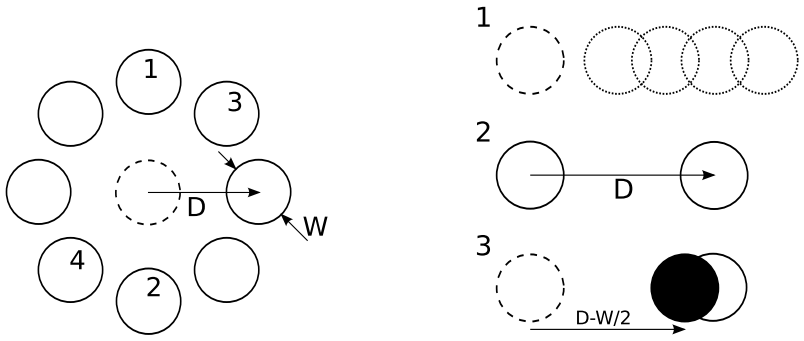

(a) ISO 9241-9 2D Task (b) 1D BCI Task

Figure 2.1: (a) An example 8 target center-out task. In this typical BCI task, the cursor is moved from the center for a distance D to a target of width W, then back to the starting target. The ISO 9241-9 standard [34], advocated for use with Fitts's Law [58], instead calls for a continuous sequence of movements to the targets in the numbered order, with no center target; movement distance varies slightly below the nominal value of $2D$ in this case. (b) Illustration of 1D pinball task sequence used in this study: (1) candidate random target positions are defined relative to (invisible) cursor before (2) target and cursor appear, and (3) cursor becomes filled once it is within $W/2$ of target center. Under a dwell-to-select paradigm, the minimum required movement distance is to the target *edge* (e.g. $D - W/2$), not center, which must be accounted for in a movement model.

Fitts's law is an empirical model developed to describe the duration of point-to-point reaching movements [22]. The model predicts movement time T as a function of movement distance D to a target of width W,

$$T = a + b \log_2 \left(\frac{D}{W} \right) = a + b\,(ID) \tag{2.1}$$

where a and b are free parameters, and the Index of Difficulty term (ID) captures task difficulty as a function of only the *ratio* between target distance and width.

The relationship, originally verified for 1D tapping tasks using a stylus [22], also describes 2D point-and-click tasks (see Figure 2.1a for example) using a computer mouse [40, 71] as well as other pointing devices. One study asserts that the a parameter should be zero after subtracting any constant (e.g. selection/click) times, and a statistical test can be used to confirm this [58].

The Shannon formulation [40] of the ID term,

$$T = a + b \log_2 \left(\frac{D + W}{W} \right) \tag{2.2}$$

is slightly different from that used in the original study. It is inspired by Shannon's Theorem 17,

$$C = B \log_2 \left(\frac{S + N}{N} \right) \tag{2.3}$$

relating channel capacity C with signal power S, noise power N, and bandwidth B [40]. We emphasize that no mathematical equivalency between the two has been established. Nonetheless, the ID term in Fitts's law is often conferred units of *bits* [18, 27] when interpreting fitting results. Throughput of a pointing device can then be specified in $bits/sec$, defined either as the inverse of the b parameter ('slope inverse method') or as the mean of ID/T over subjects and conditions ('mean of means method'); the latter is recommended in [58]. Throughput provides an attractive overall performance measure, but reporting a single number hides vital details relevant to comparing different studies. Additionally, throughput measurements of computer pointing devices show poor consistency across studies, and may have dependence on task design [58].

2.3.3 Information Transfer Rate: A Flawed Metric

In a meta-analysis following the introduction of the ISO 9241-9 standard [34], 4 studies of performance with a computer mouse at the standardized task estimate throughputs ranging 3.7-4.9 bits/sec, while 5 studies using non-standard tasks produce estimates ranging 2.7-5.17 bits/sec [58]. This demonstrates that even under the best experimental conditions, large differences in throughput-like measures across studies may not be attributable to inherent properties of the interface. For comparison, a meta-analysis of BCI studies using center-out target acquisition tasks with at least 250ms dwell times calculates the range of throughputs as 0.47-1.81 bits/sec [27], and observed between-subjects variation from 1.48-1.81 bits/sec under identical task conditions. Intracortical BCI studies frequently use only one or two subjects; in combination with the above results, this suggests that the available data best supports within-subject and within-study comparisons between manual and brain control of otherwise identical tasks.

Finally, we point out the outstanding questions and cross-purposes that exist with all claims of information quantification via movement models. A movement model can be validated on the basis of descriptive power over experimental data; it can also be related to measures of entropy from information theory. The former test is straightforward, and while it leaves room for debate as to task design and tested conditions, the range of these factors over which the model holds become a secondary validation. The relationship between movement models and information theory, however, is problematic: as evidenced by continued debate and re-analyses of the data from decades-old experiments, no mathematical *proof* or concise formulation of equivalency has been published and widely accepted. Were such a relationship established for a particular model, there remains the problem of reconciling perfect information quantification with imperfect description of experimental data: do we care about optimizing theoretical information transfer, or about optimizing observed behavior? One recent study shows, via thought experiment of sequential button-presses on a keyboard, that ID is inconsistent with entropy [59].

Fitts's law is fundamentally an empirical model, and its use and refinement here is driven by explanatory power rather than logical consistency with information theory. We refrain

from assigning units to ID.

2.3.4 Success Rates and Endpoint Distributions

Trial success rates must be high for Fitts's law to be applied to a data set, since failed trials cannot be included in the model. In tapping and point-and-click tasks, the distribution of trajectory endpoints is assumed to be normally distributed. Post-hoc calculations of effective target size can then be designed to capture 96% of all endpoints by selecting a radius of two standard deviations [40]. This approach is shown to improve model accuracy by reducing the effects of subject-to-subject variation in speed/accuracy trade-off [71].

To create a task compatible with Fitts's law and also feasible without a selection command, some studies substitute the *click-to-select* behavior with *dwell-to-select* [73]. In a *dwell-to-select* task, movement trajectories are effectively terminated when the cursor crosses the target boundary (without subsequently exiting the target). For tasks using dwell to select, trajectory endpoints are not defined in a way that easily admits similar post-hoc target width corrections.

Another important difference in the dwell-to-select paradigm is that aggressive control results in target overshoot rather than trial failure. Thus, more variability in trial times is inevitable, and success rates substantially different from 100% require explanation. If a significant number of trials fail due to reaching the trial time limit, the limit should be extended so all trials can be included in analysis, and to avoid skewing the distribution of trial times.

2.3.5 Prior BCI Studies Using Fitts's Law

Two cortical BCI studies [55, 27] and one EEG study [18] employ Fitts's law. In one cortical interface study, a point-and-click task is performed by a human with tetraplegia [55], and in the other a dwell-to-select task is performed by a non-human primate. In the study by Simeral et al., both cusor velocity and a discrete click signal are decoded from a population of recorded neurons. Because targets appear at random distances from the cursor position and multiple target sizes were used, a range of ID's were sampled that extends from less

than 1 to greater than 4. Thus, the data set permits a linear regression on ID to derive a Fitts's law trendline. It does not, however, permit the repeated-measures statistical analyses commonly used to test for data consistent with Fitts's law in the HCI community [7, 54]. To do this, it is necessary to use a discrete set of IDs with many trials conducted at each, as in [18]. Although [18] expressly sets out to validate Fitts's law in a BCI task, they use a single target width and the original formulation of ID.

In contrast to these varied task parameters, Gilja et al. use a center-out task with a single target distance and width, thus testing performance at a single ID (Figure 2.1a). In order to estimate model parameters, they assume a zero intercept of the trendline, leaving b as the only free parameter. Alternatively, this approach may be viewed as directly measuring *throughput* only, ignoring the trendline, as is advocated as an overall performance measure in [58]. Directly measuring throughput, however, assumes that Fitts's law applies to this novel task.

While the ID used in [27] is the Shannon form, the definition of D is adapted to the dwell-to-select paradigm. 'Target Center Distance' is not equivalent to 'Distance' , D, in their model; instead the substitution $D \leftarrow (D - W/2)$ must be applied to account for trajectories ending when the target boundary is crossed. This substitution makes a larger difference at smaller ID values, which are typical of BCI studies, and is therefore important. The adjustment also prevents the scenario of $D \leq W/2$, corresponding to the cursor starting already inside the target, having a nonnegative ID, as shown in Figure 2.6.

2.3.6 The Shannon-Welford Model

Although Fitts's law is widely used and shown to have excellent explanatory power over movement data, its robustness to task parameter variations is demonstrably poor. One practice which has emerged in Fitts's law studies is grouping data by either width or distance into sets which are separately fit [31]. Exploring this problem further, a recent study [54] compares the performance of Fitts's law with variants of Welford's 2-factor model [67],

$$T = a + b_1 \log_2(D) + b_2 \log_2(W) \tag{2.4}$$

which adds to Fitts's law by assuming separable gross movement and homing phases of motion. Updating Welford's model for equivalency with the Shannon form of the index of difficulty, and combining terms to match the form of Fitts's law, the Shannon-Welford model

$$T = a + b \log_2 \left(\frac{D + W}{W^k} \right) \tag{2.5}$$

is introduced in [54]. Here, k captures the effect of W on task difficulty relative to D. Note that when $k = 1$, the model is equivalent to Fitts's law. However, it is observed in [54] to take on values between 0.2 and 1.8, depending on gain - a dependence we investigate further in Chapter 3. The fact that k is often close to 1 provides insight into why Fitts's law demonstrates good fit quality in many studies. Figure 2.2 illustrates how different movement time trends can be from the times which can be captured by Fitts's law.

[54] find their variation on Welford's model to better describe manual pointing performance on very large displays, and over a wide range of control-display gains, compared to the original and Shannon forms of Fitts's law. We test whether this consistently better descriptive power carries over to isometric manual velocity control and BCI-mediated velocity control in the present study.

2.4 Methods

2.4.1 Electrophysiology

A macaque is implanted with dual 96-channel microelectrode arrays (Blackrock Microsystems, Salt Lake City, UT), bilaterally in motor cortex, connected to a 128-channel Cerebus neural signal processor (Blackrock). Manually set time-voltage criteria are used for online spike sorting, which is recorded at 30KHz for offline analysis. Custom LabVIEW software (National Instruments) is used to implement the BCI decoding algorithm and behavioral tasks. We conduct experiments in a primate behavior booth outfitted with a computer monitor, buzzers, and a computer-controlled feeder containing apple sauce. The animal's arm, contralateral to the implanted array, is situated in a custom 2-DOF near-isometric manipulandum. The computer monitor is 30 cm x 23 cm, located 28 cm in front of the

animal's head. The decoding algorithm and cursor task operate at a sampling rate of 60Hz, with the target display refresh rate 30Hz. The BCI system input-output latency is measured to be about 50ms.

The manipulandum is used for task training and to measure neural correlates of motor activity. This eliminates the possibility that neural activity is accounted for by tuning functions to limb kinematics or dynamics, since there are minimal postural changes.

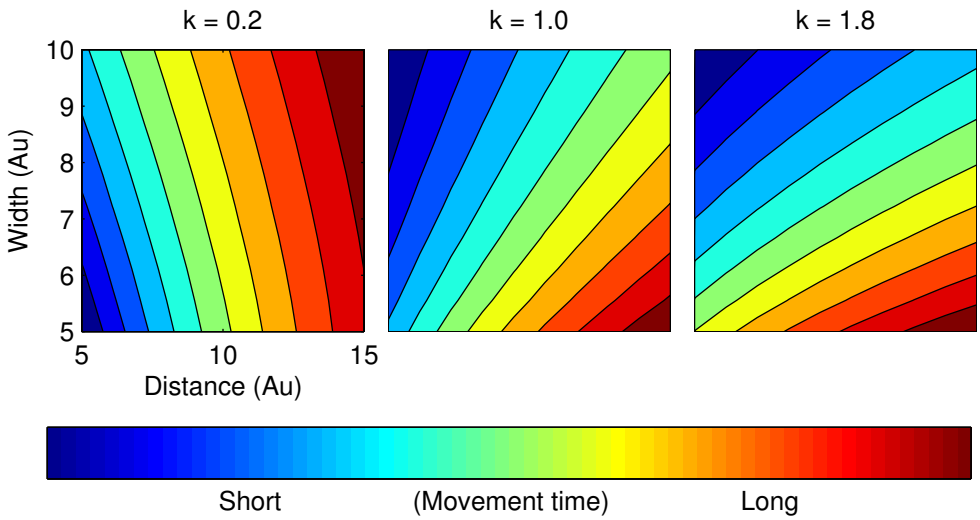

Figure 2.2: Three hypothetical plots of movement time (colored contours) vs. target distance and width, for different values of k in the Shannon-Welford model. The a and b parameters are arbitrary units (Au), held at 2 and 1, respectively, in all three cases. For $k = 1$ *(center)*, the contours of constant $\frac{D+W}{W}$ show the only possible gradient directions that can be modeled by Fitts's law. However, experimental results analyzed in [54] produced k parameter estimates ranging from 0.2 *(left)* to 1.8 *(right)*. This shows that Fitts's law is inadequate to capture the range of observed relationships between movement time, target distance, and width.

2.4.2 BCI Architecture

We implement a simple decoder based on population vector mapping [26]. For each unit, spike counts in 16.7ms bins are first filtered with a truncated Gaussian kernel, $\sigma = 0.05s$, before a baseline firing rate estimate is subtracted and the resultant instantaneous modulation estimate contributes to the population vector sum $\mathbf{u}[t]$ according to

$$\mathbf{u}[t] = \mathbf{u}[t-1] + \sum_{i=1}^{N} \alpha_i (f_i[t] - \hat{b}_i[t]) \tag{2.6}$$

$$\hat{b}_i[t] = \hat{b}_i[t-1](1-\gamma) + f_i[t]\gamma \tag{2.7}$$

where the baseline rate $\hat{b}_i[t]$ for each filtered firing rate $f_i[t]$ is continuously updated using an exponential moving average filter with decay constant γ. Modulation from each of N cells, typically $N = 4$, are summed with weights $\alpha_i = \pm 0.01$. The same algorithm is used to implement manual control tasks, where $f_i[t]$ is replaced with a torque signal and the sum is assigned to $\mathbf{y}[t]$ for direct position control.

2.4.3 Behavioral Tasks

We present the macaque with two different 1D cursor position control tasks: during manual control (MC), isometric wrist torque determines cursor velocity, and during brain control (BC), velocity is determined by aggregate cortical single-unit activity via Equation 5.2.

For a successful trial, the cursor center must be held within the target radius for 1s. Targets appear randomly, and a 1/2 second break is provided between trials. Cortical units and the direction of their mapping in the decoder are often, but not always, selected on the basis of observed correlations with torque production during manual control.

2.5 Results

2.5.1 Validating Feedback Control

We approach the problem of quantifying BCI control performance with an emphasis on describing movement times at a wide range of task geometries using well-controlled tasks. We use a manual task designed to minimize differences with the BCI task, which includes

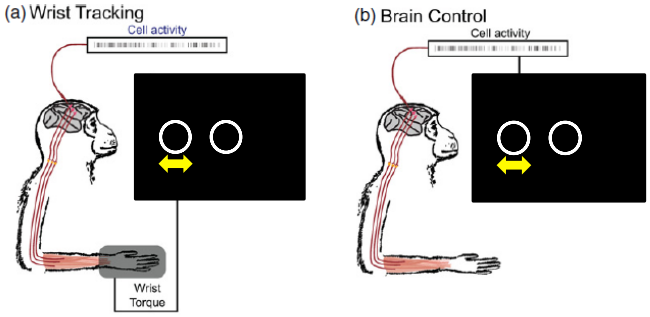

Figure 2.3: The two 1D cursor positioning tasks compared in this study. Cursor velocity is controlled either by wrist torque (left) or neural modulation (right) of up to 4 single units. The arm is in a nearly-isometric manipulandum, minimizing proprioception of limb state relevant to the task. The cursor center must be held within the target radius for 1 second for a successful trial, and a 0.5s break separates trials, during which the screen is blank. Units are selected for inclusion in the BMI based on both modulation depth and activity correlated with wrist torque.

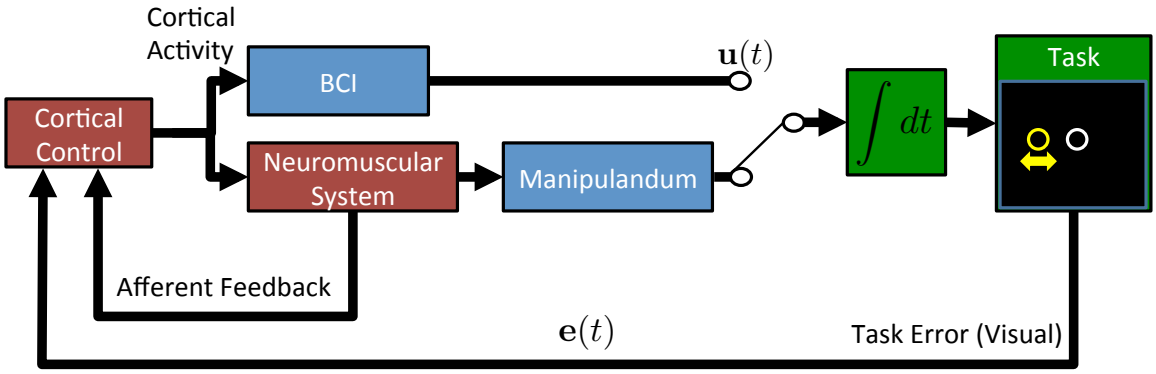

Figure 2.4: Block diagram of manual and BCI tasks used in this study. During brain control (BC), neural modulation is mapped to a 1D velocity command, as shown in the upper path. During manual control (MC), isometric wrist torque generates the velocity command. During MC, afferent feedback of commanded velocity is available. A 1D cursor control task is performed, with visual feedback of cursor and target positions.

important differences from typical reaching movement tasks: isometric force controls cursor velocity, matching the velocity control paradigm of BCI control, and minimizing proprioceptive feedback of limb position. Our use of a rate-controlled interface for manual control is unique among BCI paradigms, and specifically chosen to match the controlled system order between manual control and BCI control.

Two techniques are commonly used in BCI studies to estimate the extent to which successful trials are attributable to chance: catch trials, and chance analysis. Catch trials involve running a subset of the experimental protocol without task feedback, and possibly without other trial cues [72, 24]. The withholding of feedback and/or cues can change the subject's strategy, unless task feedback is consistently ignored. Chance analyses entail assigning probabilities to an exhaustive categorization of outcomes and require coarse assumptions, e.g. equal probability of selecting all targets [63, 52, 56]. In continuous position control tasks permitting failure, task outcomes cannot meaningfully be assigned static probabilities. A variation on chance analysis involves substituting stochastic processes or randomly-transformed copies in place of neural recordings [61]. This carries the assumption that the space of random (possibly transformed) signals is both biologically plausible and statistically representative of all possible neural signals.

We wish to control not only for chance performance, but for any target-agnostic strategy, such as sweeping the cursor across the screen. We want to reject the null hypothesis that trial success is independent of target location, regardless of reason. To do this, we use an alternative version of the catch trial which preserves experiment structure, does not sacrifice experiment time, and makes minimal assumptions about alternative possibilities to volitional feedback control. In a *simulated catch trial*, we use neural recordings to repeat experiments in simulation. We synchronize the start of each simulated trial with the start of a real trial, in order to preserve subject responses to trial start cues. This is a significant difference from [24], in which target stimuli are presented at random times during the neural activity recording. The drawback of this method is that it does not correctly capture the case where there is a non-volitional neural response to target presentation.

Targets are randomly presented in simulation, often in different locations from those in the experiment. This is very similar to the chance analysis in [37], with the notable

difference that the 2008 study used 4 or 8 discrete target locations, significantly increasing the 'chance' performance calculated if the experimental performance were good. For example, if all experimental trials were successful, then the 4-target task would produce a 25% chance success rate. In the limit of many possible target locations, the lower bound on chance success for high experimental success approaches zero. A more recent study [36] uses a similar analysis, but it is not clear whether the timing of simulated trials is locked to the timing of experimental trials. Thus, the use of a pinball task (random target locations from a non-fixed set) represents a simplifying innovation in using simulated catch trials for chance/non-volitional control analysis.

Any target-dependent task behavior, such as assistive modifications to the control signal, must be applied according to the simulated target. For example, some BCI designs attenuate movement velocity commands orthogonal to the direction towards the target by an experimenter-chosen factor [23]. A more aggressive training approach combines BCI commands with automatic target-directed velocity commands [66, 10]. This analysis can therefore be used to precisely assess marginal performance improvements even during BCI training with assisted control.

Each simulated trial is terminated when either the recorded trial ended or the simulated trial meets an endpoint condition. We treat all simulated trials reaching the end of the recorded trial without meeting an endpoint condition as failures. Importantly, the power of this analysis depends on the number of different possible target locations in each trial.

The results of this catch trial analysis are shown in Figure 2.5, reflecting the average of 100 simulations of each trial. The histogram of successful trial times, and total success rate, can be compared to that of the original experiment. Comparing the trial time histograms of simulated catch to real trials, we can see that the strong majority of successful trials are not attributable to target-agnostic performance. We thus eliminate the possibility of significant successes attributable to *any* target-agnostic control strategy, of which chance success is a subset.

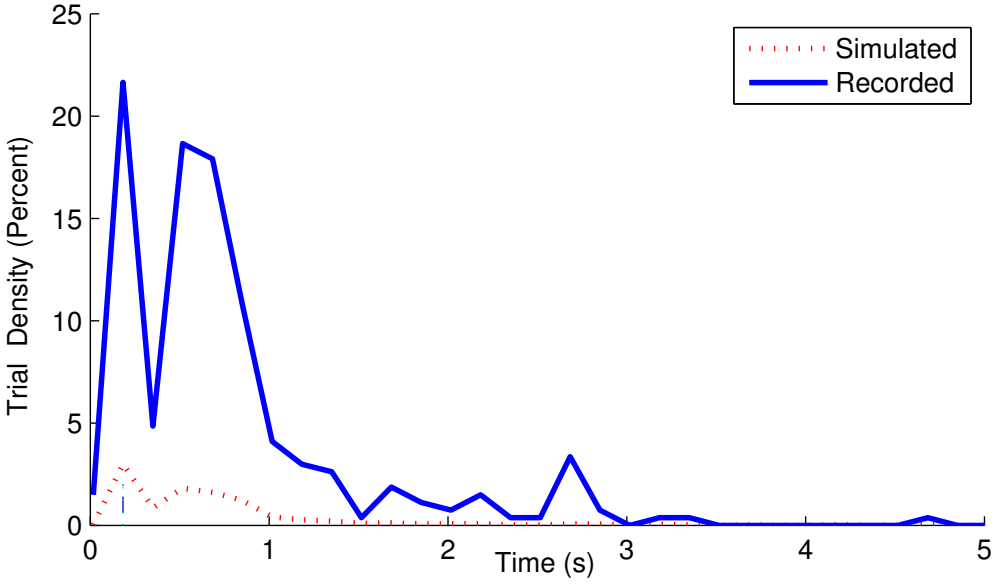

Figure 2.5: Simulated catch trials from 2013-01-14 compared to experimental data via trial-time histogram. We subtract the simulated, potentially target-agnostic, successes from the actual histogram as a worst-case assumption. Failed trials are not shown; in experimental data they result only from a time-out condition, whereas in simulation, some trials terminate without success or failure because the recorded trial ended before the simulated one. We perform this analysis for the easiest target geometry in particular to confirm that it is not too easy. The magnitude of simulated successes is much less than recorded successes. This confirms that the likelihood of success with a target-agnostic strategy is not high enough to substantially affect results.

2.5.2 Model Fitting

We begin with a sample analysis of brain control trials from one day, shown in Figure 2.6. From this process we learn that trial time distributions under constant conditions are better described by a log-normal than a normal distribution. We confirm this choice by assessing the normality of residual modeling errors with and without the log transform using Q-Q plots, shown in Figure 2.7. Consequently, all fitting is done to log movement times.

We next establish under what circumstances the Shannon-Welford model significantly outperforms Fitts's law. We examine 41 experimental day $\times$ condition data sets to test the power of both Fitts's law and the Shannon-Welford model. The pool of data sets considered have at least 500 trials including 2 unique D and W values, and a significant model fit ($p \leq 0.05$) for at least one of our candidate models. To each data set, we apply the Shannon-Welford (eq. 2.5) and Fitts's law models (eq. 2.1). Because the Fitts's law model is equivalent to the Shannon-Welford model if $k = 1$, an F-test of nested models can be applied to determine whether the added parameter is justified by significantly improved explanatory power [14].

We find that the Shannon-Welford model is significantly better for 10 of 18 (55%) manual control data sets ($p \leq 0.05$), and for brain control we find it to be better for 15 of 23 days (65%, $p \leq 0.05$). Decomposing these results by the number of distinct target widths used in each data set suggests that at least 3 widths should be used to realize the benefit of the 3 degree-of-freedom Shannon-Welford model (Figure 2.8).

On six experimental days, more than 500 trials of both manual and brain control were conducted, and we focus on these days for more detailed analysis of fitting results. A summary of the experimental conditions and results is shown in Table 2.1. We can see that values of the k parameter are generally within the range seen in studies of other interfaces [54], and show significant day-to-day variability.

Finally, we show model fit surface plots along with prediction intervals for brain and manual control on each day in Figure 2.10 . These plots show that while the identified models cannot demonstrate a consisently significant difference between brain and manual control on a given day, they can suggest trends which may become significant with lower-variability trial times. Critically, the results are only valid for the task geometries tested, which is why our surface plots only extend to the smallest rectangle bounding the test conditions. The suggested trends include that distance plays a dominant role in determining difficulty (consistent with $k < 1$), and that brain control tasks take substantially longer at higher difficulty levels. For a single quantitative measure, we could evaluate the gradient magnitude in the center of these fitted surfaces, bearing in mind that this measure would be biased by our choice of experimental conditions.

Figure 2.6: Model fitting process for brain control trials on 2013-03-01. First, we convert from center-to-center target distances to center-to-boundary distance by substituting $D \leftarrow D - W/2$, eliminating the region where the cursor's starting position is inside the target boundary. Next, we test trial-time distributions for normality and log-normality using the Lilliefors test, revealing that log-normal assumptions are more consistent with the data. The $D \times W$ conditions with the greatest numbers of trials are shown, with colors corresponding to the width vs. distance plots, and bold lines or filled markers indicating conditions where trial times did not fail a Lilliefors test of log-normal distribution. Finally, we apply the Shannon-Welford model to $\log(T)$, and plot the fitted surface with the individual trials.

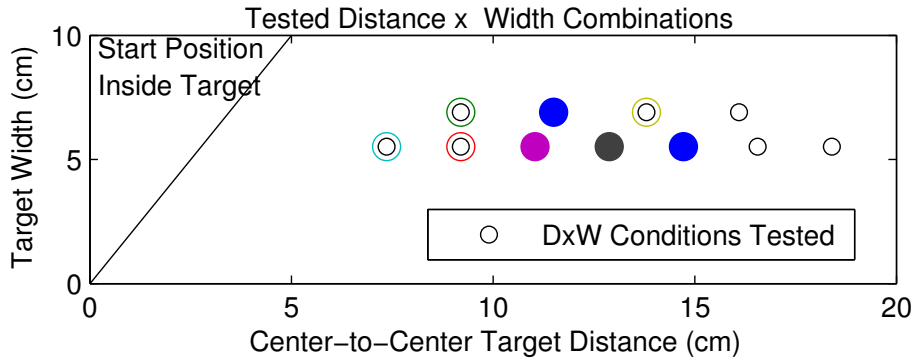
Tested Distance x Width Combinations
Start Position
Inside Target
DxW Conditions Tested
Target Width (cm)
Center−to−Center Target Distance (cm)
0
5
10
15
20

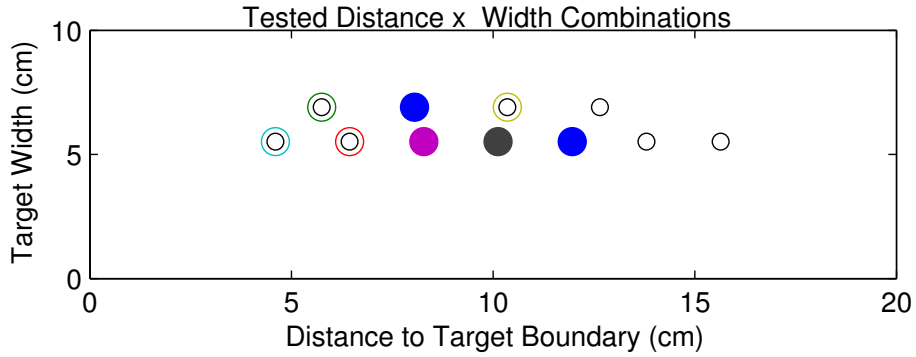
Tested Distance x Width Combinations
Target Width (cm)
Distance to Target Boundary (cm)
0
5
10
15
20

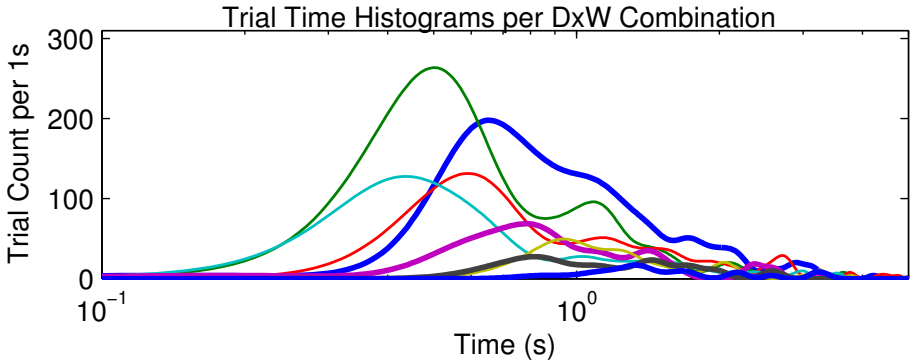
Trial Time Histograms per DxW Combination
Trial Count per 1s
Time (s)
300
200
100
0

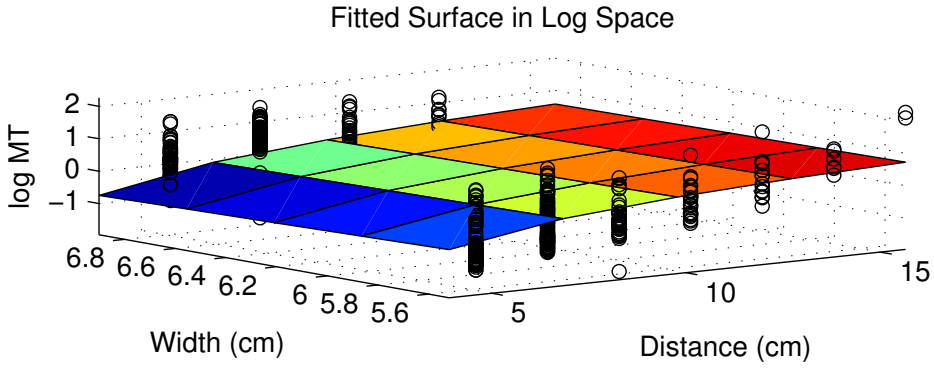
Fitted Surface in Log Space
log MT
Width (cm)
Distance (cm)
2
1
0
−1
6.8
6.6
6.4
6.2
6
5.8
5.6
5
10
15

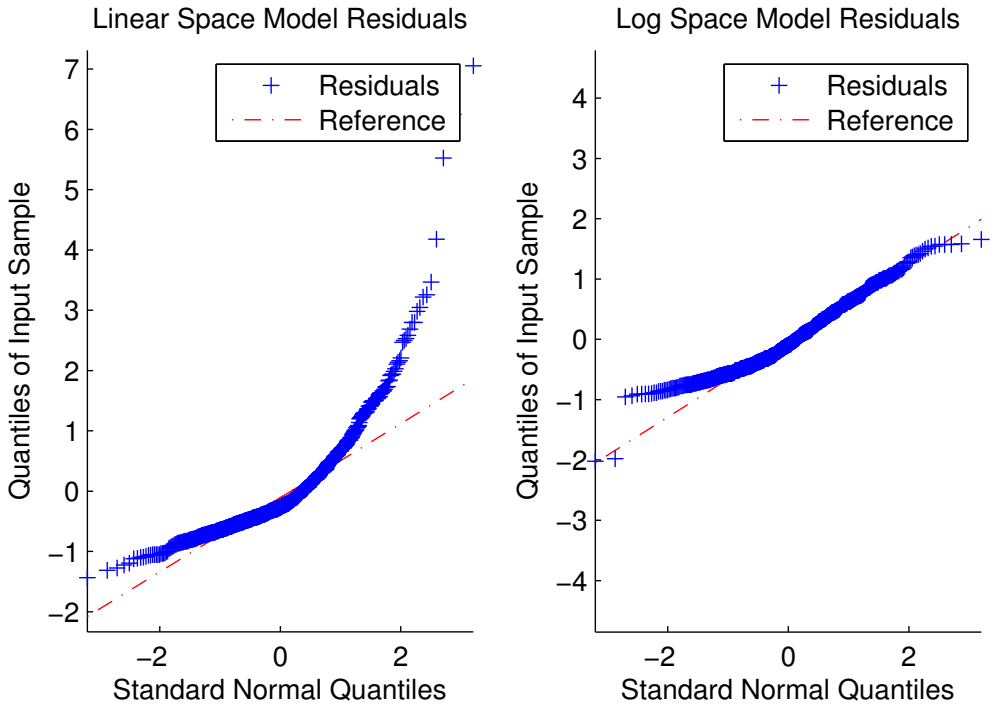

Figure 2.7: Quantile plots of residual model errors for brain control trials on 2013-03-01, providing a comparison of the residuals (blue crosses) to the normal distribution (red lines). Residual errors more closely align with a normal distribution for the log-transformed model, confirming that this transform should be used.

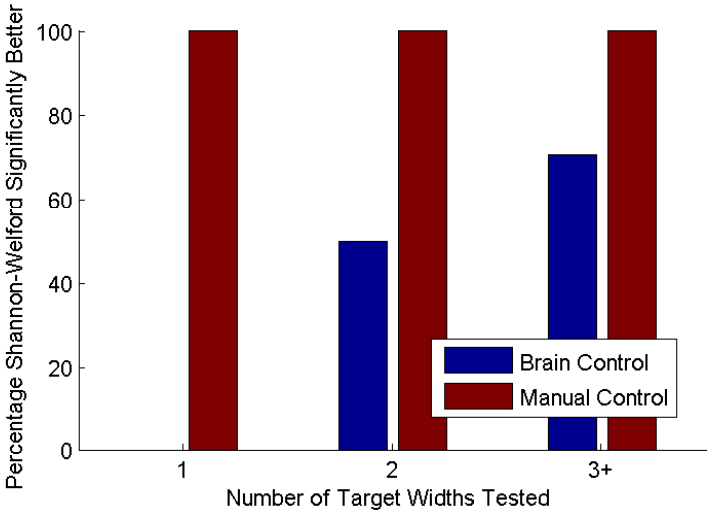

Figure 2.8: Shannon-Welford model performance relative to Fitts's law, as a function of the number of distinct target widths used. The nested models F-test is used to determine whether the Shannon-Welford model significantly outperforms Fitts's law for each data set [14]. This aggregate plot shows that multiple target widths are required for the more complex model to provide benefit. The same is likely true of distances, but we always used several target distances. The modeling results represented here include all days having at least 500 trials under the condition (Manual, Brain).

2.6 Discussion

2.6.1 Summary of Results

We reviewed prior work in the use of empirical movement models as performance metrics for pointing tasks, including recent works demonstrating critical flaws in the Fitts's law model, and establishing superiority of the Shannon-Welford model.

We next provided methods to address uncertainty about the volitional control involved in experiments. For model fitting, we showed that for this dwell-to-select task with non-proficient performance, trial times are best assumed to have a log-normal distribution rather than a normal distribution. We then showed that the Shannon-Welford model best describes movement times in reaching tasks controlled manually as well as directly by cortical activity,

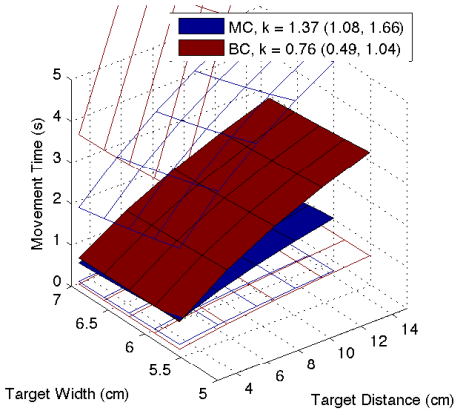

(a) 2013-02-20

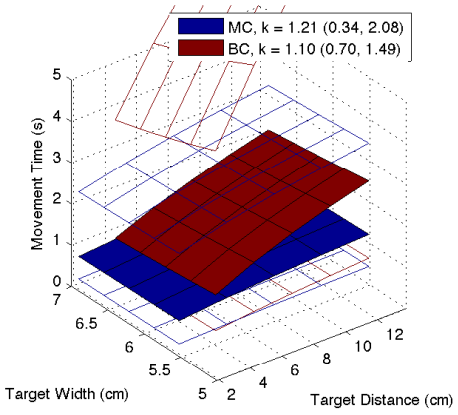

(b) 2013-02-26

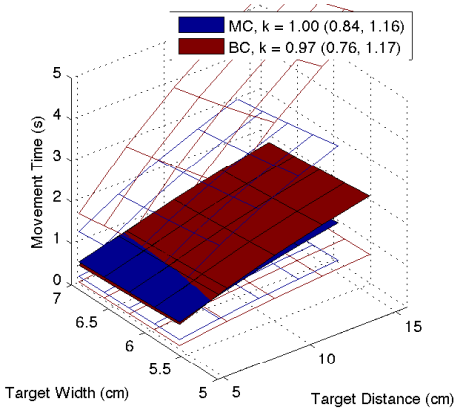

(c) 2013-03-01

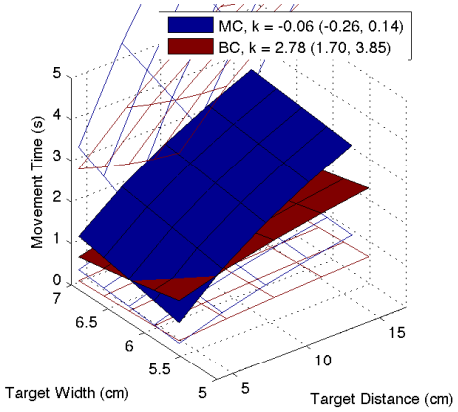

(d) 2013-03-21

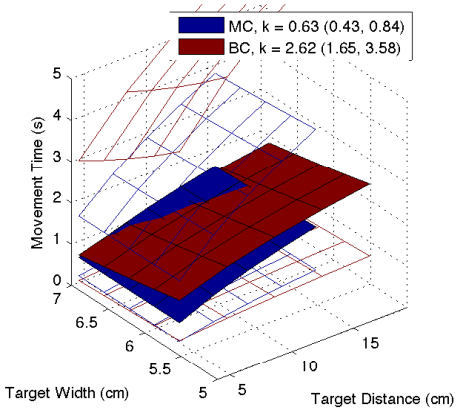

(e) 2013-03-22

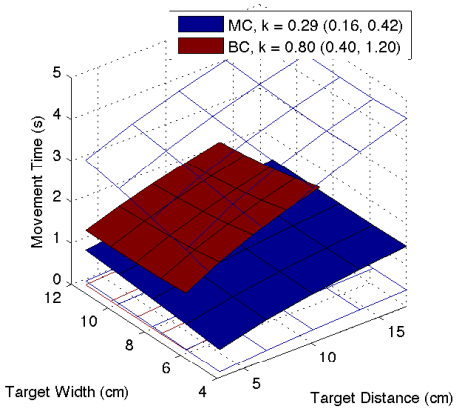

(f) 2013-11-20

Figure 2.10: Comparisons of identified models of movement time between manual and brain control, for six days on which significant data sets were collected for both manual and brain control. Surfaces show model fits, while open grids show prediction confidence intervals (95%). We can see that the confidence intervals are too large to determine significant differences between brain and manual control.

outperforming the incumbent Fitts's law. We believe that these methods for evaluating data quality and fitting a descriptive model of movement control can provide a framework for thorough evaluation of BCI performance and equitable comparison across studies.

2.6.2 Dwell Time

Although not incorporated into the movement models considered here, dwell time is a critical factor in BCI task design. Our approach is based on the intuition that long enough dwell time requires similar position stabilization as is used when selecting targets via explicit command (e.g. clicking). With short dwell times and during poor cursor control, we expect dwell time to affect movement times, and we chose dwell time to explicity avoid this situation. In this study, we chose a dwell time of 1s, which we believe is high enough to prevent a strategy of 'drifting' across the target in an uncontrolled way. A standardized dwell time, such as 500ms, may minimize potential confound in future studies. In addition, there is evidence to suggest that the importance of dwell time will diminish as user proficiency improves. A study of eye-tracking for 2D cursor task control [73] finds that movement times vary less than 5% between dwell requirements of 500ms and 750ms (recall that dwell is not included in selection time). A simple way to avoid the confound of dwell time in 2D interfaces is to use crossing-based tasks, which are shown to have movement times consistent with Fitts's law [1].

2.6.3 Trade-offs Unique to BCI Experiments

In developing summary recommendations for BCI task design, we are keenly aware that each trial performed with a BCI utilizes precious experimental time and subject motivation. The 8- target center-out and pinball tasks are the dominant incumbents, while the IS0 9241-9 is the gold standard for manual control. While switching to the ISO task may not yet be justified, researchers can replicate its properties of near 180-degree direction reversals, no breaks between trials, and exact knowledge of the next target position when designing the next generation of BCI tasks.

While we are sensitive to the limited experimental time available to test both animal and

human BCI performance, we recommend the use of at least 3 distinct distances and 3 distinct widths of target – with the largest possible separation – to determine the Shannon-Welford model fit. Simulated catch trials are recommended, particularly for the least-difficult task geometries, to confirm volitional and target-dependent control.

2.7 Conclusion

Our goal in adapting a movement model for BCI-mediated tasks is to enable comparison with native motor control. As more advanced BCIs enable more control degrees of freedom (DOF), movement models based only on *task* DOF may seem inadequate if the number of controlled (e.g. manipulator) DOF exceeds the task degrees of freedom. However, this is exactly the context in which a task-based model can reveal similar performance trade-offs between BCI and native control. In a native motor task, we expect task difficulty, and consequently movement times, to increase with task DOF, despite the *control* DOF (e.g. the arm) remaining exactly the same - and grossly larger than the task DOF. We expect to see this dissociation between task and control degrees of freedom in proficient BCI use.

A simple thought experiment can tell us what performance tradeoffs are likely to look like if the user cannot simultaneously control all degrees of freedom. Imagine measuring movement times for a 1D task and a 2D task, first with controlled degrees of freedom equal to task degrees of freedom. With native control, we expect 2D tasks to be slightly slower [71]. With nonconcurrent control, however, we expect 2D tasks to take at least twice as long as 1D tasks, because a 2D task is tantamount to two sequentially-performed 1D tasks with the additional challenge of multi-DOF dwell.

Extending this to over-actuated systems (having more control DOF than task DOF), we expect an additional controlled degree of freedom to slightly decrease movement times under proficient control, but to significantly increase movement times under nonconcurrent control. Nonconcurrent control may describe not only BCI control, but also a native motor task combining controlled degrees of freedom in a novel way. In particular, this may be the case when only a selected or classified subset of control DOF is active at each instant, such as is the case with some myoelectric prostheses.

We acknowledge the frustration at the loss of a single quantitative performance measure,

but emphasize that the failure of consistency between studies, in addition to the logical inconsistency of information claims, compel the community to find a better standard measure than Fitts's law.

Movement times well-explained by a movement model are a necessary condition to claim performance tradeoffs on par with the native motor system in pointing tasks. However, sufficient conditions for parity with manual control may be as diverse as motor tasks. We expect that a BCI system well-integrated into the subjects motor schema will incur similar movement time penalties as the native motor system when task degrees of freedom are increased. This may be easier to assess than acquiring an exhaustive sampling of task geometries.

We advocate a focus on comparing direct neural control performance to native limb movement, under otherwise identical tasks and controlled system properties. Conducting such experiments under the broadest feasible range of task parameters will maximize information about the limits of speed/accuracy tradeoffs and shortcomings of the neural control interface, informing directions for further investigation and innovation.

Manual Control Results

Day	D levels	W levels	DxW levels	Trials	R^2	k	F-test
2013-11-20	9	5	37	857	0.16	0.83 (0.72,0.95)	p=0.015
2013-03-01	8	2	9	908	0.20	1.00 (0.84,1.16)	p=0.988
2013-03-21	7	2	14	511	0.28	-0.06 (-0.27,0.14)	p=0.000
2013-03-22	7	2	13	1002	0.20	0.63 (0.43,0.84)	p=0.002
2013-02-26	10	2	14	1121	0.09	0.68 (0.45,0.92)	p=0.007
2013-02-20	10	2	14	991	0.16	1.37 (1.08,1.66)	p=0.005

Brain Control Results

Day	D levels	W levels	DxW levels	Trials	R^2	k	F-test
2013-03-01	10	2	11	730	0.16	0.97 (0.76,1.17)	p=0.747
2013-02-20	12	2	13	636	0.14	0.76 (0.49,1.04)	p=0.093
2013-02-26	10	2	13	613	0.05	1.10 (0.70,1.49)	p=0.619
2013-11-20	9	5	34	571	0.03	0.80 (0.40,1.20)	p=0.422
2013-03-22	9	2	17	716	0.13	2.62 (1.65,3.58)	p=0.000
2013-03-21	8	2	15	654	0.16	2.78 (1.71,3.86)	p=0.000

Table 2.1: Detailed summary of fitting results for subset of 6 days: those meeting the prior criteria of at least 500 trials, and at least 2 distinct distances and widths, for *both* brain and manual control. The number of DxW levels is not equal to the product of the D and W levels tested because the study is unbalanced. This is due to screen geometry constraints and the distribution of randomly-generated targets. Due to large trial time variation under constant task conditions, R^2 values are poor; instead, parameter confidence intervals on identified parameters should be used to judge fit quality. Additionally, the ultimate utility of applying these models is in assessing the difference between two fits. We report $k(\pm 95\% CI)$ because it relates to the difficulty trade-off between small targets and large distances. Nested models F-test results in rightmost column show in which cases the Shannon-Welford model is significantly better than Fitts's law.

Chapter 3

PERFORMANCE CONSEQUENCES OF CONTROL-DISPLAY GAIN

3.1 Chapter Summary

In Chapter 2, we showed that the Shannon-Welford model applies to visual BCI tasks, outperforming the Fitts's law model. In this chapter, we use the Shannon-Welford model to shed new light on existing experimental results in pointing device control. We provide new insight by analyzing movement tasks in the coordinate frame of the input device instead of the frame of the visual display. The scaling factor between a user's movement and movement on a computer screen is the basic adjustment that can be made to improve pointing device performance. Extending this concept to novel interfaces, including BCIs, we consider the general question of how control-display (CD) gain affects performance. Control theory can provide an answer to this only if given a model of the user as a controller. Here we take an empirical approach, investigating the implications of the movement model we used in Chapter 2. We investigate the affect of CD gain on performance, with the goals of separating out drivers of difficulty and of informing cross-device interface performance comparisons. We show the separable effects of the motor task (or command signal generation) and of the visual feedback scaling on performance. We also dig deeper into the relevance of the k parameter in the Shannon-Welford model, which captures the relative effects of target distance and width on task difficulty. Building on the finding in [54] that the k parameter has an affine relationship with gain, we provide evidence that $k = 1$ may correspond to conditions of maximal performance and ease-of-use. While multiple studies of the effect of CD gain on movement exist, they do not yield gain selection principles generalizeable across interface modalities. Finally, we propose that k values can be compared across interfaces, instead of gain, because this unit-free quantity captures the functional consequences of gain.

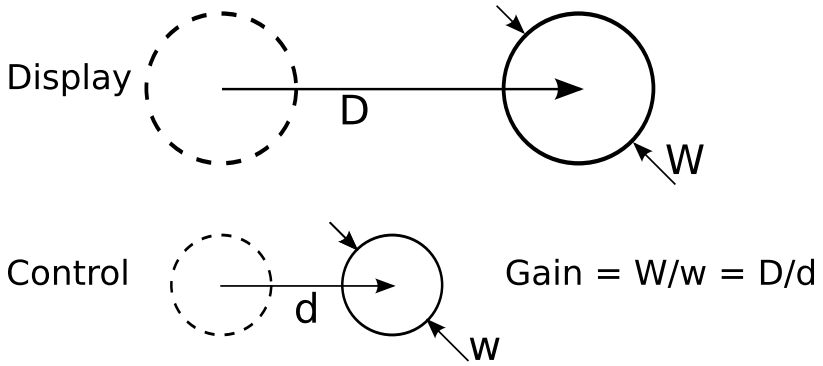

Figure 3.1: Illustration of a cursor positioning task represented in *control space* and in *display space*, showing that control-display (CD) gain corresponds to the geometric scaling factor between these two representations.

3.2 Introduction

In Figure 3.1, we illustrate how control-display (CD) gain relates the scaling of displayed task feedback to underlying motor (or command) task. As we explain below, this relationship exists even when no physical movement is involved in generating a movement command, such as when neural activity mediates movement control. Also, instead of a constant gain, a non-linear mapping may exist between the two spaces. In fact, consumer pointing devices for computers make heavy use of *pointer acceleration* functions which are highly non-linear [5], and this technique has also been applied in the BCI context [66]. Here, we restrict our analysis to simple scalar gains.

In this section, we first explain the unique importance of choosing CD gain for BCIs. We next present specific hypotheses about the effects of CD gain on performance and provide background on how BCI gain is reconociled with decoding algorithms based on state estimators. Then we review prior work in selecting BCI gain, and in selecting CD gain for manual force regulation studies. We conclude the introduction with a review of the Shannon-Welford model, the empirical model of reaching movements upon which our analyses are based, and its implications for how CD gain may affect performance.

3.2.1 The Dual Control Problem in BCIs

The successful use of a Kalman filter, or other linear estimator, in a control system is predicated on the *separation principle*, which allows an optimal state estimator to be designed separately from an optimal controller. In order to design either, the system dynamics must be known – in the case of a BCI, the dependence of cortical activity on kinematic state and visual feedback of error. Thus arises the *dual control* problem [17], wherein the problems of controlling a novel system and perturbing it to identify its dynamics are inseparable. If a system can be modeled using additive Gaussian noise (or no noise) and linear dynamics, and costs are quadratic, then the design of an optimal controller and estimator can be performed separately; absent these conditions in the BCI context, the two design problems must be addressed as a whole. This problem is implicitly and sub-optimally addressed by co-adaptive BCI paradigms, which reveal an additional problem: cortical dynamics are time-varying. While the use of linear dynamic models is known to be a coarse but tolerable approximation, time-varying system parameters must be explicitly dealt with. This is commonly accomplished by either repeating the parameter identification process completely at a regular interval [55], or by iteratively updating the parameter estimates with marginal adjustments to reconcile inconsistencies with the most recent data [66, 47, 27]. Howover, it has been shown that the separation principle does not apply in this case of time-varying stochastic linear systems [64], but adaptive control solutions exist [65]. Consequently, an opportunity exists to improve the closed-loop dynamics of BCI control systems via gain selection.

3.2.2 Hypotheses

We begin with the intuition that performance differences between pointing tasks with the same visual geometry, but different CD gains, may be accounted for by the different scales of physical movement required - i.e., the scale of the underlying *motor task*. For example, if CD gain is increased by 10×, we hypothesize that requiring one-tenth the tolerance of motor control is the dominant cause of increased movement times. This implies that the brain is able to perfectly compensate for the ratio (CD gain) between physical movement

and visual feedback. Therefore, the alternative is that this ratio causes variable difficulty for the same physical movement.

To test this hypothesis, we must separate the influences of motor task scale and CD gain on performance. The studies we review do not do this, so we must determine whether this information can be extracted from the experiments that were conducted, and whether such separation is possible in general. This leads to a more fundamental question: are there separable impacts of CD gain and motor task scale on performance?

Fitts's law has been used, with relative success, to explain published experimental results for the past five decades. Yet, recent studies show it to hold only under a restricted set of conditions [54, 31]. Our intuition is that these conditions, where $k = 1$ in the Shannon-Welford model, are self-selected by researchers or subjects. We hypothesize $k = 1$ to represent optimal conditions, but lack a cost function known to capture optimality criteria. Subjective ease of use and movement time are the measures available to us to test hypotheses. The complete set of hypotheses we will test is as follows:

- H1: CD gain and control task scale have separately measureable impacts on movement task durations.

- H2: Control task scale, and not CD gain, is the dominant cause of movement duration changes.

- H3: A value of $k = 1$ in the Shannon-Welford model correlates with maximizing both objective performance and subjective ease-of use. We define the gain (and k value) of maximum performance as that which minimizes movement times, relative to other gain choices, over the largest range of tested task geometries.

After reviewing prior results on control-display gain in BCI and motor tasks, we analyze several experiments to address the above questions. We conclude with some suggestions on improving experiment design to address the questions rasied here, and on optimizing BCIs used for visual control tasks.

3.3 Background

3.3.1 Movement Models

We draw upon two movement models, both developed to describe the time of rapid, aimed reaching movements. Fitts's law and the Shannon-Welford model both describe tasks which can be parametrized by target distance, D, and width, W. While Fitts's law uses only the ratio D/W,

$$T = a + b \log_2 \left(\frac{D}{W} + 1\right) = a + b\,(ID) \tag{3.1}$$

the Shannon-Welford model [54] incorporates each parameter separately in accounting for movement times,

$$T = a + b \log_2 \left(\frac{D + W}{W^k}\right) \tag{3.2}$$

$$= a + b_1 \log_2 (D + W) - b_2 \log_2 (W) \tag{3.3}$$

and is shown to better explain movement data. The second representation helps show the separable effects of distance and width assumed by the model. These separate terms are attributed to a movement phase, possibly ballistic, followed by a homing phase [67]. Based on our work, and that of Shoemaker et al, we use the Shannon-Welford model here.

3.3.2 CD Gain for BCIs Based on State Estimators

Defining control-display gain for BCI contexts can be confusing, because one decoding paradigm is to estimate intrinsic movement state variables assumed to be encoded in cortical activity. The state variables capture the features of either imagined or actual limb movement which is linked to cursor dynamics on the display.

Consequently, the design goal of the decoder can be thought of as perfectly estimating movement parameters which are represented on the visual display, such as during manual task control. Were a decoder to achieve this, logical consistency would require the control-display gain to be unity (possibly after a transformation from limb kinematics to cursor coordinates). While the decoder and visual display may be an imperfect state estimator from

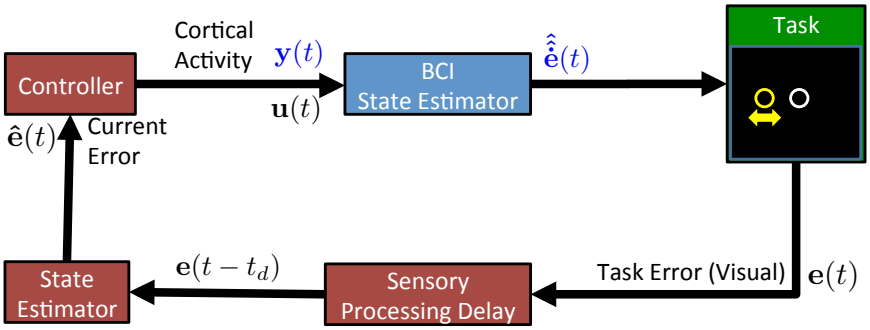

Figure 3.2: This block diagram of a closed-loop BCI shows the conflict between the brain's control task and the assumptions behind a BCI decoder designed as a state estimator. Black signal labels show names consistent with the brain's point of view, while blue labels show the state estimator's assumptions. The signal $\mathbf{u}(t)$, which is the control input to an unknown plant for the brain, is treated as the output $\mathbf{y}(t)$ of a system whose state is to be estimated by the decoder. Then, a subset of the estimated state – the derivative of position error, i.e. velocity command/observation – becomes the task input. We abuse notation to denote that the task command is an estimate of an estimate of cursor position error.

the designer's point of view, from the brain's perspective the decoder is a dynamic system which mediates control of visual feedback tasks. These dual and conflicting perspectives are illustrated in Figure 3.2. Within this feedback loop that includes the brain, a de facto gain is applied to the decoded signal in representing it on the display.

Decoders are trained, meaning parameters are chosen, by fitting to neural activity recorded during manual movement or during observation of cursor control. Importantly, the fitting process entails assumptions about the subject's internal representation of both physical movement parameters and intended movement parameters. The set of assumptions implemented in the fitting algorithm, and the set of movement conditions (such as ballistic motion vs. 'homing' on a position), both influence resulting changes to the decoder and de facto gain.

For example, Figure 3 in [47] shows large changes in the estimated neural tuning function amplitudes for a small population of neurons. Assuming a consistent level of state estimation

performance, decoder gain is unchanged. But from the brain's perspective, these changes represent dramatic gain changes in the decoder, since the contribution of each neuron to the decoded command is weighted using its tuning amplitude. Similarly in [55], gain is implicitly set by construction of a Kalman filter for estimating encoded velocity. In the next section, we review studies in which gain selection is an explicit experimenter choice, because the decoder algorithm was not a state estimator.

3.3.3 Examples of BCI Gain Selection

A number of approaches have been used to choose BCI gain, either to maximize performance or to enhance learning [23] . In some cases it is chosen without detailed explanation, such as [9], where it is termed *speed factor*. One study used increased gain in conjuction with an 800ms task completion deadline to incentivize more ballistic movements [62]. Another used a "non-linear gain function designed to suppress low speeds and amplify high speeds" [66], similar to a mouse acceleration profile. In general, formal methods have not been used to choose CD gain to maximize closed-loop performance.

3.3.4 Prior Results in Force Control with Visual Feedback

Prior studies of isometric force control under different visual feedback gains reveal significant effects on performance. In [12], the authors conducted an isometric force-matching task simulating braking in a race car, with race car drivers as subjects. The results show that control-display gain "had large effects on build-up speed, overshoot, within-participants variability, and self-reported physical load." The optimization problem is characterized by the authors as achieving the best trade-off between physical effort and stability.

The authors of [57] conducted an isometric force-matching task using the index finger of several subjects. A graphical strip-chart representation of force production on a computer screen provided feedback on instantaneous force as well as the time history of force during the current trial. Each trial entailed matching a reference force, set as either 5% or 25% of maximum voluntary contraction (MVC) of the subject, and provided as a reference line on the computer screen. Control-display gains spanning a range of 250 were used, and

subjects of widely varying ages were included to reveal age-dependance of performance curves. The relationship between coefficient of variation (CV) of force and control-display gain exhibited a U-shaped curve, implying a performance-maximizing CD gain near some middle value. The curve was more pronounced at the higher percentage of MVC. This is important, because it suggests that making large changes to the scale of a task in motor space will affect performance, independent of any changes to visual feedback scaling. These two studies make it clear that control-display gain, in isolation, has some effect on feedback performance in force-modulation tasks with zero-order dynamics.

This suggests that the same may be true in movement tasks, but this must be verified separately because the dynamics are different: compared to zero-order direct force control, cursor control tasks are more often rate-controlled (first order), which is the case for most BCI decoders, or approximately second-order with many nonlinearities, in the case of controlling natural reaching. In Section 3.4, we review and analyze the results of gain optimization studies of such systems.

3.3.5 Display Space and Control Space

We distinguish measurement of movement parameters in *display space*, defined as the embodiment of the task provided as visual feedback to the user, from measurement in *control space*, the parametrization of control action by the subject. *Display space* is visually observable to the subject, whereas *control space* may be observable only e.g. via proprioception, or not at all. For physical, non computer-mediated tasks, such as positioning a stylus, these two frames of reference are the same [22]. In a computer-mediated task, however, the task space is the display, and the control space can be mouse position, (possibly integrated) joystick force, or any measured biosignal. In prior work using Fitts's law and similar models, mathematical models of movement describe performance in task space [40, 58, 6, 7, 54]. The choice of coordinate frame for describing task geometry has significant consequences, as we show later in this chapter.

3.3.6 Thought Experiment

The recent study which validated the Shannon-Welford model found that CD gain and the k parameter have an affine relationship with positive slope: as gain increases, the relative importance of target width in determining task difficulty increases as well [54]. It is intuitive that at very low gain, movement to the target will dominate task duration, whereas at very high gain, settling time to a precise endpoint location will dominate and in the limit of very high gain, make the task impossible.

While varying CD gain often changes movement duration, re-scaling the task can (under specific conditions) be perfectly compensated for. For example, imagine an interface with gain chosen so that $k = 1$. Consider halving control-display gain while preserving visual task geometry, compared to doubling the visual task scale but keeping control-display gain constant. In the latter case movement time will be invariant, but in the former we will change k, and consequently may change the movement time prediction. Both have the same task geometry in control space, and consequently admit the same optimal control trajectory. However, one varies the relationship between motor action and visual feedback, and the other does not. This motivates our investigation of how CD gain affects performance of the same underlying control space task.

3.4 Re-Analysis of Movement Studies

We consider the question of performance-maximizing gain selection in a novel way: given a fixed (range of) display task scale, we have one constraint on the coupled variables of CD gain and control space task. We can pose the following question: for a given control-space task geometry, what CD gain results in the lowest movement time? From this perspective, the visual representation of the task serves the purpose of providing feedback to the user, and CD gain allows us to choose the visual scaling which optimizes performance of the underlying (e.g. motor) control task. In other words, what is the scale of control task and feedback amplification that the brain is inherently best adapted for? Once we have solved this problem, we can add the objective of matching display task scale to a real workspace. This contrasts with display-focused approaches to adjusting CD gain, in which keeping the

display task invariant while adjusting CD gain changes both the underlying motor task and the visual feedback scaling. It is with this in mind that we approach re-analyzing the results of a few recent pointing interface studies, all of which correlated CD gain with movement time at fixed display task geometries. In this section we review three studies of computer-mediated movement control: one using a conventional mouse, one using a very large display with gesture control, and a third using a rate-control interface with variable stiffness.

3.4.1 Movement Control on a Large Display

In [54], human subjects stood in front of a wall-sized (3m x 5m) display and perform a 1D positioning task in which horizontal motion of a handheld object was mapped to horizontal cursor position. CD gain was varied from 2-20, and movement times were measured at nine different combinations of three distances and three widths, covering a regular grid in the distance-width parameter space. Analyzing the movement times using the Shannon-Welford model they introduced, the authors identified parameters for display space models of movement time at each gain. While they identified the trend in k vs. CD gain and established the robust descriptive power of their model, they did not visualize the 3D surfaces embodying their models.

We begin our analysis by visualizing movement time as a function of target distance and width in display space, as shown in Figure 3.3a. Intersections between these surfaces represent boundary conditions where switching to a different gain can lower movement times. If we extrapolate beyond the grid of experiment parameters, the model fit surfaces converge just beyond the lowest tested target width of 50mm. A single surface representing achievable movement times by choosing among the gains is shown in Figure 3.3b, revealing that the highest gains minimize movement time. However, by extrapolating the surfaces beyond $W = 50mm$, we reveal a graded transition in optimal gain as a function of target width. Thus, large regions of task geometry exist for which either the highest or lowest CD gains minimize movement time, and a much smaller region exists in which intermediate CD gains minimize movement time.

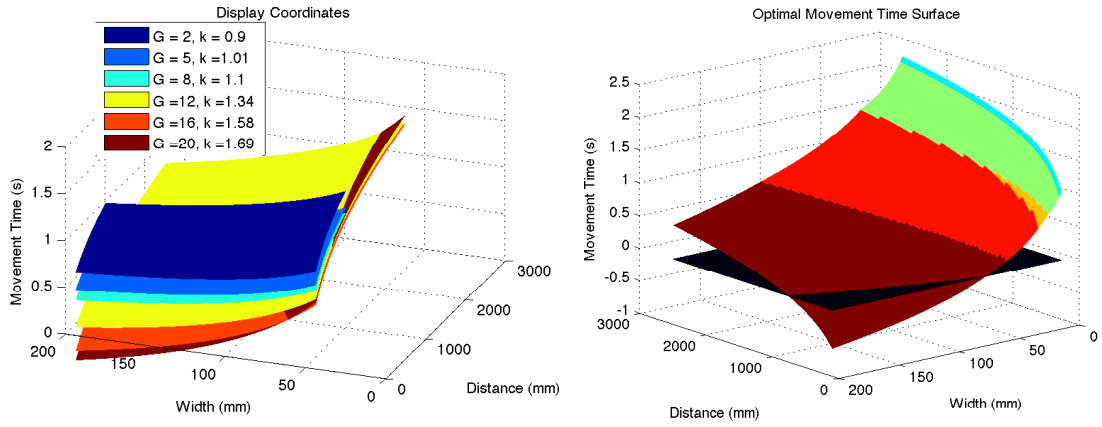

(a) (b)

Figure 3.3: (a) Shannon-Welford model fits predict movement time (vertical axis) as a function of target distance and width in display space at different CD gains. The largest distances could not be tested at the lowest two gain values. (b) Hypothetical minimum-time surface in display space, defined as the minimum achievable time if gain be selected based on task geometry. The surface is colored based on selected gain, and extrapolated beyond the smallest experiment-supported target width of $50mm$. Dark plane at $T = 0$ delineates regions of implausible movement time predictions *within* the region of experimental support, despite model goodness-of-fit of 0.98 (for gain of 20).

3.4.2 Hypothesis Testing

If *control* task scale is the driver of task difficulty, then tasks of identical motor geometry but different display geometry should have identical movement times. To test this, we transform the task geometries from *display space* to *control space*, as shown in Figure 3.4a. In control space, the tested task geometries provide only partially overlapping support for movement time predictions, shown in Figure 3.4b, limiting possible performance comparisons among CD gain selections. We also see that extrapolation not far beyond the data-supported regions results in implausible movement time predictions (e.g. negative times for larger target widths at high gain).

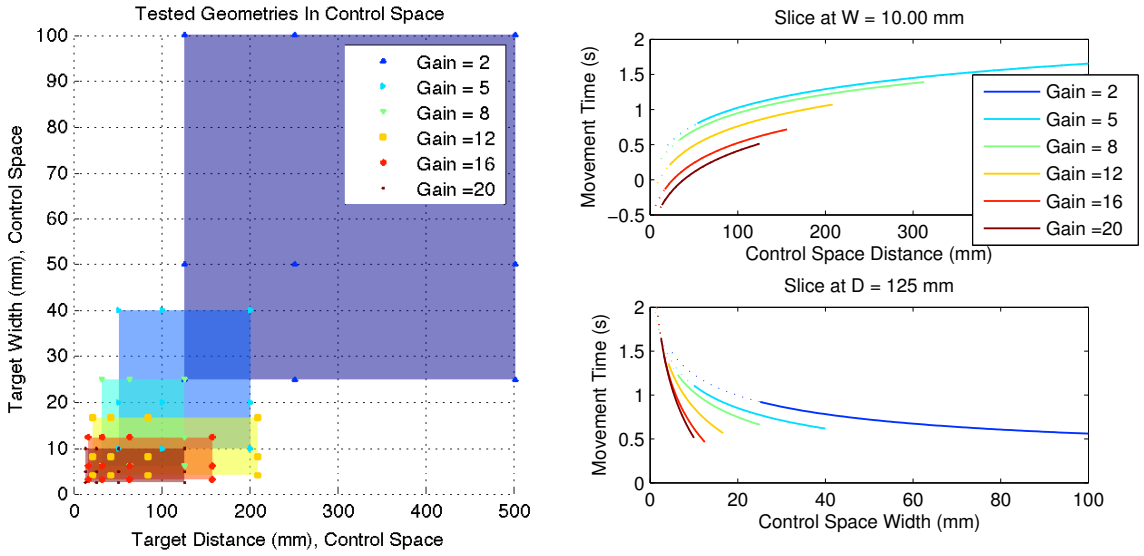

(a) (b)

Figure 3.4: *(a)* Task geometries in control space at each CD gain tested: points are tested conditions and shading is supported model fit range. While the set of tested task geometries is the same at each gain in display space, they comprise partially-overlapping regions in control space. *(b)* Movement time predictions in control space vs. width *(bottom)* or distance *(top)* variation only. Dotted lines indicate model predictions extrapolated beyond experiment geometries (black dotted line at $D = 0$). Model fits in control space, illustrating difficulty of comparing model fits: gains tend to be predicted optimal at target geometries outside supported range.

Some important pieces of information can be drawn from the *control space* analysis. First, varying CD gain at constant control space geometry affects movement time, compelling us to reject H2. This is evidenced by different movement times at the same control space $D \times W$ conditions. Second, the analysis of Figure 3.4b effectively separates the effects of CD gain and *control* task geometry, consistent with H1.

3.4.3 Ease-of-Use

We have discussed the minimization of movement times, our basic performance indicator, but we have not addressed the definition or conditions of optimality. While Shoemaker et al do not propose any objective assessment of optimality in their study, they do survey subjects about subjective difficulty of the different gain settings. Low (2,5) and medium (8,12) gains are scored as the easiest and second-easiest, in stark contrast to the result that higher gains minimized movement times. This suggests that a cost function determining control strategies is elevated under high gain conditions. Additionally, the preferred gains corresponded to k parameter values closest to 1. Our extrapolation of the minimum-time surface in Figure 3.4(b) predicts that the gain at which $k = 1$ is optimal for most geometries with target width less than 50mm. This suggests that reported difficulties would be different if the *maximum* target width were 50mm, and that the use of movement time as a peformance measure is influenced by the experimenter-chosen task geometry. Consequently, it may be possible to repeat this study with fully contradictory results on preferred gain and time-minimizing gain, by choosing target widths $\leq 50mm$.

3.4.4 Rate-Control Interface

We next examine a study conducted with an elastic rate control interface at different levels of stiffness as well as CD gain [6]. Casiez et al used a Phantom Desktop haptic device to simulate an elastic 1D rate control interface with different levels of both stiffness and gain. The interface mapped force to cursor velocity, with the exception of a zero-stiffness condition, under which position was mapped to velocity. Subjects performed a 1D positioning task on a standard-size computer display.

The application of Fitts's law to recorded movement times at each gain $\times$ stiffness combination shows poor goodness of fit ($R^2 < 0.80$) in 10 out of 25 conditions. Figures 3.5(a-b) show Shannon-Welford curve fitting results at the highest stiffness condition, repeating the time-optimization CD gain analysis as in the previous section. The lowest R^2 value for the Shannon-Welford model across all conditions in this study is 0.923. This shows that the superior explanatory power of the Shannon-Welford model extends to rate-controlled

interfaces as well as direct position control interfaces. This is consistent with our results in Chapter 2, and substantially stronger due to the high goodness-of-fit for a data set including 21600 trials from 16 participants.

3.4.5 Relationship of k vs. Gain

We can derive the dependence of k on CD gain separately at each stiffness level, resulting in the linear affine fits shown in Figure 3.5(c). The same relationship as observed in [54] holds for rate-controlled interfaces, albeit with poorer goodness of fit. The slope of this trendline increases monotonically with stiffness. Under the assumption that increasing k corresponds to increased settling time relative to ballistic movement, this implies that endpoint stabilization is degraded at higher stiffnesses, when less displacement is involved. This is consistent with an explanation that prioprioception is a performance-limiting feedback signal for this task. If this explanation is correct, it suggests that the slope of the k vs. gain curve will be greater yet for EMG interfaces and BCIs, since there is no proprioceptive feedback at all in those cases.

3.4.6 Time Minimization

Figure 3.5(b) shows the minimum-time performance surface for the Casiez study at the highest interface stiffness condition. The gain corresponding to $k = 1.04$ minimizes movement times over a majority of the task geometries supported by experimental data in this case, providing an interesting contrast to the results of the Shoemaker study. In fact, at all four non-zero stiffness conditions tested by Casiez et al, the gain(s) corresponding to k values nearest 1 minimized movement time over the majority of the experimental task geometries. To represent this aggregate trend across stiffness conditions, we plot the fraction of task geometries for which a value of k is time-minimizing in Figure 3.6(a). For three of the four non-zero stiffnesses, the k value nearest 1 minimizes movement time over the largest range of task geometries. Bearing in mind that these results are driven by the choice of task geometry, we wonder what shift in tested geometries would change the outcome for the two low-stiffness conditions inconsistent with this trend.

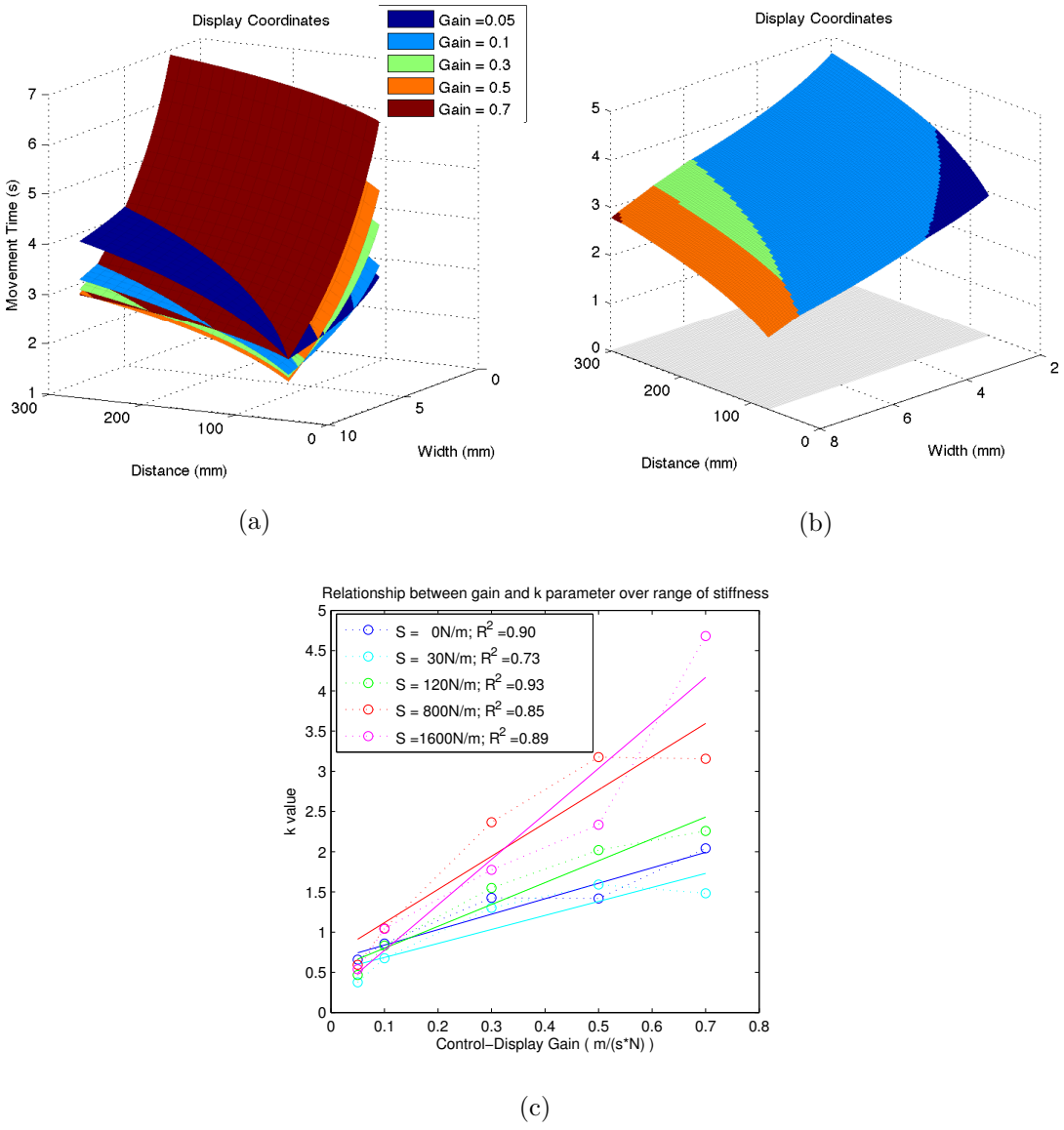

Figure 3.5: The display-space analysis of movement time surfaces is repeated for this study *(a)*, generating the minimum-time surface *(b)*. The minimum-time gain analysis is aggregated across all stiffness conditions in Figure 3.6. In *(c)*, we show the dependence of k on gain at each stiffness condition. This shows a trend in the slope of this relationsip as a function of stiffness.

In summary, CD gains minimizing $|k-1|$ also minimize movement time in most cases. This result supports H3 for performance maximization, with the caveat that the result depends on the task geometries tested. The study also reports subjective ease-of-use using relative comparisons between sequential CD gain levels. This is combined with subjective evaluations from all studies in Section 3.4.7.

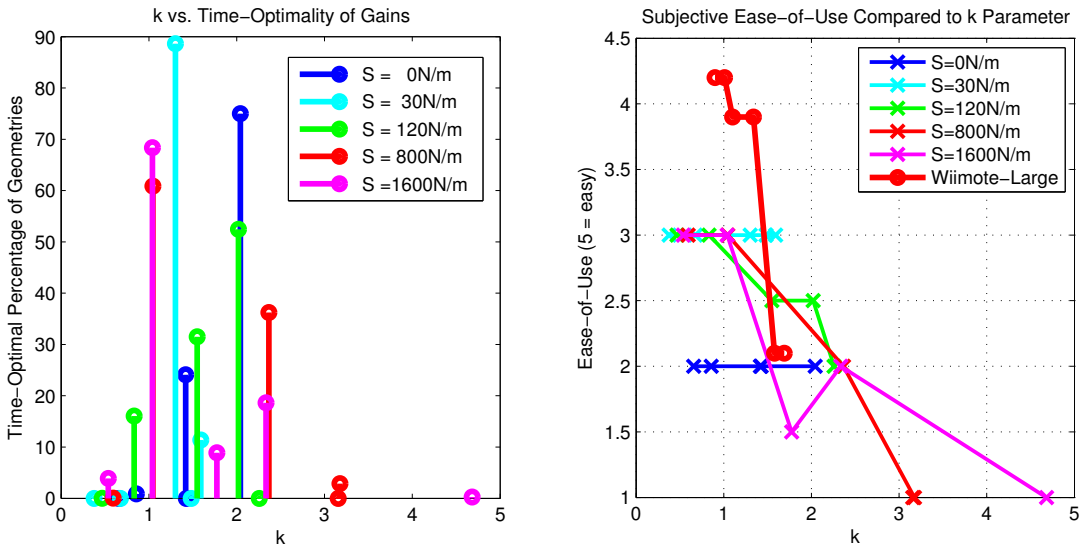

(a) (b)

Figure 3.6: (a) At each stiffness, we calculate the percentage of task geometries for which each CD gain is optimal. We then map CD gains to identified k values. This supports that k values near 1 minimize movement times. (b) Reported ease-of-use of interface as a function of k, compiled from 3 different studies. The first five legend entries are different stiffness levels from [6], followed by [54]. Reported ease of use is maximized where $k \leq 1$ across all studies.

3.4.7 Optimality Criteria

Movement duration is thus far used as the condition-specific performance metric. It can be averaged to provide an aggregate measure across task geometries, similar to the throughput

measure advocated for use with Fitts's law [58]. However, recall that throughput measure is biased by the range of ID values – driven by task geometries – tested in an experiment. Replacing Fitts's law with the Shannon-Welford model exacerbates this problem by adding a second degree of freedom to the experimenter-chosen parameters influencing the metric.

Distinct from performance is optimality, which must incorporate control cost as well as performance. Energy is not minimized in e.g. arm movements [38], so in considering the optimization of movement control, the cost assigned to effort cannot be assumed constant across task difficulties. In fact, evidence to the contrary exists in a study of deadline-based arm movements [2]. In that study, subjects increase effort via cocontraction to maintain performance as required accuracy increases. We must therefore allow the possibility that control effort varies with task geometry, control gain, and any other manipulated variables. Yet, we have little justification for any optimality measure other than reported ease-of-use. Any other choice imposes external cost weightings on the subject.

In Figure 3.6(b), we show reported ease of use as a function of k for both studies discussed above, as well a third which involves a conventional computer mouse [7]. The mouse study records control performance over a range of gains with a normal sized computer display, then repeats the experiment with a very large display (4.7m x 1.7m). A noteworthy feature of the large display experiment is that significant clutching, or interrupting movement to physically re-center the mouse, is involved at lower CD gains. However, the Shannon-Welford model describes this data with surprisingly good results. The condition $k \leq 1$ captures nearly all peaks in user preference for the ensemble of experiment results.

3.5 Discussion

3.5.1 Review of Hypotheses

We sought to test three hypotheses in our re-analysis of pointing interface data sets:

- **H1:** CD gain and control task scale have separately measureable impacts on movement task durations. **Result: not rejected.** Multiple distinct model fit surfaces visible in Figure 3.4b support this hypothesis.

- **H2:** Control task scale, and not CD gain, is the dominant cause of movement duration changes. **Result: rejected.** This is rejected by the same evidence in Figure 3.4b, clarifying that the first two hypotheses are incompatible with each other.

- **H3:** A value of $k = 1$ in the Shannon-Welford model correlates with maximizing both objective performance and subjective ease-of use. **Result: not rejected.** However, the available data is incomplete and noisy, and further investigation is warranted.

A step towards understanding optimality conditions, we showed that users prefer CD gains corresponding to a k value near 1. However, the empirical data provided here is insufficient to determine a specific value or confidence interval for a preferred value of k. In particular, the preference vs. k curves had maxima at lower range boundaries in some cases. More information about user preference for $k < 1$ is needed.

3.5.2 Summary of Other Novel Findings

The pointing interface tasks we have considered here can be parameterized by their geometry, either in display space or in control space, and the interface gain. The studies we reviewed made comparisons of movement times across CD gains with tasks parameterized in display space. This obscures the separable relative contributions of CD gain and control space task geometry that we hypothesized to exist. Our analysis of the study data in control space revealed non-overlapping task geometry ranges at different gains, limiting possible comparisons from this perspective. This can be partially solved by testing smaller task geometries – both distance and width – at low gains. Thus, one outcome of our analysis is showing that experiments could be designed to better test the effect of CD gain across the control space. This issue also highlights the importance of reporting the scale of physical movements or signal amplitudes required of the user to fully describe a pointing device experiment.

Extending results in [54], we showed that the Shannon-Welford model applies to a rate-control interface as used in [6]. Specifically, it outperforms Fitts's law in describing movement times at variable gains, and the k parameter has a linear affine relationship with gain,

as Shoemaker et al observed with the same model applied to two direct position control interfaces.

3.5.3 Relevance to Current and Future Research

In the two experiments with large displays, the experimenters expect poor ease-of-use due to the unsolved optimization problem of cursor control on large-format displays. Interestingly, in one of these, the conditions we claim to be optimal lie outside the range of tested conditions. In a novel interface, there could be a mismatch between the optimal task geometry range and the needed range of operation. If these regions are different, we have what appears to be conflicting optimization needs. Depending on the application, one candidate solution is to separate control-display gain from control-*task* gain. Examples from teleoperated robotic manipulation may be instructive. Several recent studies of robotic surgery tasks have addressed gain selection problems for robotic surgery [51, 15], including one which explored variations in both display gain (optical zoom) and control-task gain.

We do not address the problem of choosing optimal CD gain for learning, but this is a useful direction for further investigation. In a kinarm reaching experiment with a rotational mapping distortion, error offsetting provided fastest learning and error amplification produced the most complete learning [8].

Our results, particularly with the variable-stiffness rate-control interface, motivate investigation of similar tradeoffs in BCI design: we expect that the k vs. CD gain slope will be quite large due to the complete lack of non-visual feedback. [61] shows that providing kinesthetic feedback via passive movement of the subject's arm significantly improves performance. Consequently, providing afferent feedback of either position or commanded velocity may produce substantial performance gains.

Finally, we propose a possible standardization of approach in characterizing and comparing novel control interfaces. Investigators should identify the k vs. Gain trendline for a novel interface, and select the gain for which $k = 1$ to measure performance that is comparable to other (e.g. incumbent) devices. Simply adjusting gains so that the k values are equal will, for lack of a rigorous argument that such comparisons are 'fair', allow comparisons

between interfaces to be made based only on the two remaining parameters in the Shannon-Welford model. Moreover, seeking conditions where $k = 1$ may provide an optimization approach that is robust across many interfaces and improves performance more efficiently than guess-and-check approaches.

3.6 Future Work

Our results motivate further investigation of what conditions *optimize* an interface in terms of performance/effort tradeoff. An interesting experiment would be to let users periodically adjust CD gain during a set of position tasks, and examine the choice of gain as a function of the experimenter-chosen task geometries. As we have framed the optimality question, this experiment would answer how k is related to optimal gain.

The rate-control interface study we reexamined repeated experiments at multiple levels of stiffness, and found that the slope of the k vs. gain trendline is greater at higher stiffnesses. To account for the slope increase of the k vs. gain relationship with increasing interface stiffness, we proposed that this is attributable to decreased proprioceptive feedback. Under this assumption, we raise the question: what sets an upper bound on the k vs. gain slope for interfaces completely lacking proprioception, such as EMG or BCI? Further, can the k vs. gain slope be considered a measure of the quality of feedback available to the subject? A meta-analysis or a novel experiment design may be able to answer this question.

Finally, we have not made a distinction between display scaling measured as physical size vs. as visual angle. It would be very interesting to find out if there are separable effects of these two, such as by moving a computer display relative to the subject but not changing the display scaling.

Chapter 4

APPLYING BEST PRACTICES FROM DIGITAL CONTROL SYSTEMS TO BCI IMPLEMENTATION

4.1 Chapter Summary

Many brain-computer interface (BCI) algorithms, such as the population vector decoder, must estimate neural spike rates before transforming this information into an external output signal. Often, rate estimation is performed via the selection of a bin width corresponding to the effective sampling rate of the decoding algorithm. Here, we implement real-time rate estimation by extending prior work on the optimization of Gaussian filters for offline rate estimation. We show that higher sampling rates result in improved spike rate estimation. We further show that the choice of sampling rate need not dictate the number of parameters which must be used in an autoregressive decoding algorithm. Multiple studies in other neural signal processing contexts suggest that BCI performance could be improved substantially via careful choice of smoothing filter, discrete-time decoder representation, and sampling rate. Together, these ensure minimal deviation from the behavior of the modeled continuous-time systems.

4.2 Introduction

Brain-machine interfaces mapping activity of well-isolated neurons or multiunits in cortex have shown promise for allowing the continuous control of robotic limbs and computerized assistive devices [32]. Original single-neuron BCI experiments required the use of analog circuitry to implement low-pass filters for neural spike rate estimation [19]. This was an encumbrance that limited design flexibility. As recently as 2004, studies investigating the effect of sampling rate on digital BCI performance were limited by the available computing hardware [68]. Enabled by ever more compact and powerful computing hardware, contemporary algorithms for converting the recorded activity of large populations of individual

neurons into movement commands are increasingly complex, drawing on tools from control theory and machine learning such as Wiener Filters [68, 45], Support Vector Machines [60, 24], and Kalman filters [35, 39, 25]. Sampling rates for the digitally implemented dynamics of these systems remain as low as 10 Hz [39, 48, 4, 3]. By comparison, modern action-oriented computer games typically refresh the screen at 30 Hz or above and simulate underlying game physics at even higher sampling rates in order to achieve a sense of realism.

Many BCI architectures implement spike rate estimation and decoders such that the behavior of both is driven by the choice of a shared sampling rate. This need not be the case. Consequently, there is an opportunity for improvement by increasing sample rates that has been overlooked thus far.

Our use of the term *decoder* refers broadly to the mathematical transform between spike rate estimates and BCI output signals, and is inclusive of transforms which do not attempt to literally decode limb movement.

Here we demonstrate three advances. In Section 4.3, we show that the use of a Gaussian smoother with optimized bandwidth outperforms the time-bin (histogram) method in spike rate estimation. In Section 4.4, we discuss the benefits of high sampling rates and illustrate with an example of spike rate estimation performance. In Section 4.5, we show the benefits of choosing a model with the minimum number of parameters to capture dynamics. Finally, in Section 4.6, we describe how down-sampling can be used to implement such a model with a high sampling rate.

4.3 Spike Rate Estimation with Smoothing Filters

Spiking neurons are well-modeled as inhomogenous Poisson processes, making it possible to estimate the underlying time-varying distribution parameter using a variety of methods [53]. The vast majority of BCI designs estimate instantaneous neural firing rates by counting the number of spike events in a temporal bin, with widths typically in the range of 30 to 100 ms. This histogram process is equivalent to two separate steps: filtering using a rectangular kernel, then sampling with a sample period equal to the kernel width. This is illustrated in Fig. 4.1.

This simple method produces an estimate because, for a time-invariant Poisson process,

the expected number of events in a given time interval is proportional to the distribution parameter. This estimate is still rather noisy, and in some designs is fed into another moving average filter [68, 45].

The rectangular kernel can be replaced with an arbitrary kernel function, and the sampling rate need not be the inverse of the kernel width. Shimazaki and Shinomoto (2009) developed an algorithm for selecting the optimal width of a given symmetric kernel function by minimizing the mean integrated square error (MISE),

$$MISE = \int E(\hat{\lambda}_t - \lambda_t)^2 dt \tag{4.1}$$

between the rate estimate and unknown underlying rate [53]. Their algorithm utilizes sample data as a proxy for the statistics of unknown rate λ_t to optimize rate estimate $\hat{\lambda}_t$.

They showed that using a Gaussian kernel significantly outperformed the histogram method when both had widths optimized for offline spike rate estimation. Their performance comparison of different rate estimation methods using synthesized neural recordings is shown in Fig. 4.2. The Gaussian kernel is also an attractive choice for real-time applications because it has minimal rise and fall time with no overshoot. For a more in-depth discussion of methods of spike rate estimation, see [11].

The optimization algorithm generates the optimal kernel width for a specific data set. Therefore, to find the kernel width best suited for a particular BCI application, a data set which captures neural firing statistics during BCI operation is needed.

Moritz and Fetz (2011) showed that modulation depth of neural firing can vary substantially between tasks performed manually and under single-neuron BCI control by macaque monkeys [43]. This means that optimizing a kernel based on recorded data prior to BCI control may not result in good performance under BCI control. To bootstrap the system, we can use a data set recorded during manual tasks or while the animal is at rest. Once data recorded during BCI control is available, a sufficiently large duration of recordings should be used to capture the full range of firing behavior and re-select the optimal kernel bandwidth. Fig. 4.3 shows the resultant MISE cost functions for neural firing recorded from the same neuron under different conditions. We can see that the cost function is relatively flat for a wide range of kernel widths, regardless of recording context. In choosing a kernel

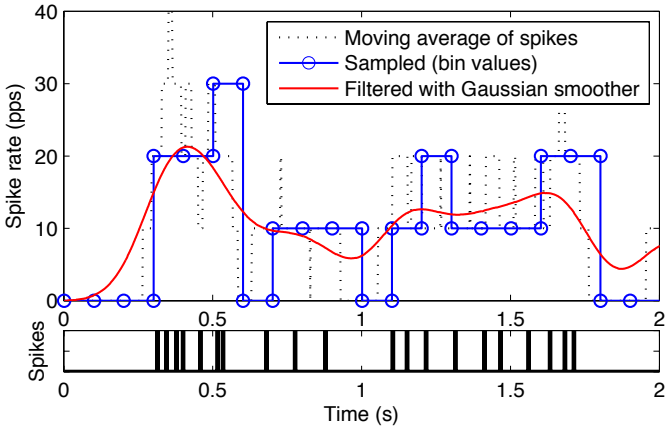

Figure 4.1: Illustration of the two underlying components of the histogram spike rate estimation method: filtering with a rectangular moving average, followed by sampling with sample period equal to window width, 100ms. For comparison, the output of a Gaussian smoothing filter with $\sigma = 100$ms is shown as well.

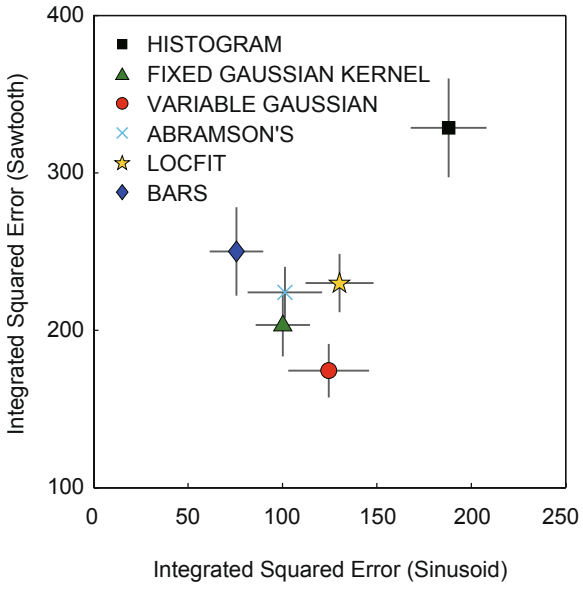

Figure 4.2: Performance comparison of six rate estimation methods based on MISE when applied to synthesized data with sinusoidal and sawtooth underlying rate functions. Modified from [53].

width for better robustness, an experimenter can select one that may not correspond to the global minimum for the most recent data set, but will result in an acceptable MISE. As a low-pass filter, the Gaussian smoother places limits on the bandwidth of the entire BCI system and also introduces a delay, creating an incentive to choose the smallest kernel width that results in an acceptable error. The threshold near zero width at which the cost function begins to increase dramatically is fairly consistent among recording contexts, indicating that a kernel width near this threshold should continue to perform well as neural modulation changes with BCI use. Thus, firing rate estimation variance can be robustly reduced by the replacement of a histogram estimator with a Gaussian smoothing filter. Gaussian kernel smoothing is optimal in terms of both *latency* and firing rate estimation accuracy compared to other moving-window smoothing filters, and no more computationally demanding in on-line implementation than the rectangular filter. In Section 4.4, we address the digital implementation of a Gaussian filter.

4.4 Digital Implementation of Dynamic Systems

Multiple rules of thumb exist for selecting a sufficient sampling rate for the discrete-time representation of a dynamic system. In order to avoid aliasing (signal artifacts that result from too low a sampling frequency), the signal must be sampled faster than the Nyquist rate. The Nyquist rate is defined as two times the bandwidth, or maximum frequency, of a signal or dynamic system response. The Nyquist rate represents an absolute *lower bound* on sampling rate for reconstruction of the original signal or system dynamics; sampling at or marginally above this rate, as is sometimes done [68, 39], does not result in *good* reconstruction up to the bandwidth frequency. In fact, it is desirable to sample 10 or more times faster than the bandwidth, because this factor represents the number of sample points used to represent one cycle of a sinusoidal signal.

For example, Figure 4.4 illustrates the effect of sampling rate selection on the MISE associated with a Gaussian filter sampled at different rates and truncated at $\pm 2\sigma$ in order to reduce latency. Gaussian filters have a cutoff frequency of $1/\sigma$ where σ is the standard deviation of the kernel, making the Nyquist sampling rate $2/\sigma = 10$Hz in this example. We can see that MISE is significantly improved at a sampling rate of 60Hz, which is 12 times

the bandwidth.

We have chosen an appropriate sampling rate for a Gaussian filter based on an application-specific criteria, without regard to the bandwidth of the incoming spike train. In general, it is essential to select a sampling rate which captures the full bandwidth of the input signal as well as the dynamic response of the system. This will be our approach to implementing the decoder following the rate estimation filter.

By virtue of being the solution to the rate estimator optimization problem, the bandwidth of the Gaussian filter provides an upper bound on the bandwidth of the firing rate estimate signal. More information may exist in the spike activity, but we implicity ignore it as noise. We maintain the sampling rate of 60Hz for the decoder, and in the next section we address the system identification problem of literally decoding limb movement.

4.5 Model Selection

Dynamic models are often used to decode limb movement from neural firing, and subsequently to map neural firing to BCI output signals. Moving-average architectures such as the Wiener filter have been widely used [45, 3], and more recently Kalman filtering methods based on state-space models have gained popularity [39, 11].

The block diagram in Fig. 4.5 illustrates the system identification problem for decoding limb movement. Consider the frequency-domain transformations from the spike train $S(s)$ to $U(s)$ and $Y(s)$,

$$\begin{aligned} U(s) &= F_i(s)S(s) \\ Y(s) &= F_o(s)G(s)S(s) \\ \frac{Y(s)}{U(s)} &= G(s)\frac{F_o(s)}{F_i(s)} \end{aligned}$$

We can see that in order for the relationship between the recorded input $u(t)$ and output $y(t)$ to be equal to the unknown transformation from neural spiking to limb movement $g(t)$, the two filters in the recording pathways, $f_i(t)$ and $f_o(t)$, must be identical. Although this approach appears to discard information from the output signal, remember that the smoothing filter implicitly considers signal energy above its bandwidth to be noise. Note

that we are sampling a tiny subset of the neural activity driving low-level control of muscle recruitment. Therefore, it is possible that the spike rate signal has higher bandwidth than observable from gross limb movement dynamics. We can bound the bandwidth of the dynamics relating neural firing rate to limb movement by the bandwidth of the observed output signal, limb trajectories during motor activity.

If we measure limb movement with no filtering, the system identification algorithm will see an incorrect very high gain on these high-frequency signals, and the resultant model will attempt to amplify the high-frequency signals that the rate estimation filter is designed to eliminate. Therefore, although the recorded limb trajectory will likely have higher bandwidth than the spike rate estimate, it should be filtered in the same way as the raw spike train because higher frequency signal energy will not improve the model. In order to build a higher-bandwidth model of the relationship, it would be necessary to obtain a higher-bandwidth input signal, such as by incorporating the firing of additional neurons.

In selecting a model architecture either for directly transforming neural activity or for use in a Kalman filter, it is important be aware of the implications of the model structure and of the number of free parameters. Specifically, a higher number of model parameters will be required to capture higher-order dynamics, but this requires substantially more data for a fitting algorithm to arrive at good parameter estimates. Therefore, the experimenter should choose a model with the minimum number of parameters required to capture the dominant dynamics thought to exist in the system. Autoregressive moving average (ARMA) models have been shown to perform well among other linear models [21]. A dynamic system of a given order can be modeled with less parameters with the ARMA structure than via a state-space or impulse-response formulation.

4.6 Decoder Implementation

Because a small number of model parameters will be fit to a large data set with noise, the sampling rate of the model must be chosen so that the dynamics capture the underlying system behavior while ignoring the noise. This motivates the selection of a sampling rate only a few times greater than the bandwidth of the *signal* content of the recorded data. The bandwidth of limb trajectories and the optimal kernel bandwidth both suggest choices

for the model bandwidth. To convert the 60 Hz sampled signal from the smoothing filter to, for example, a 10 Hz dynamic model (Nyquist rate of 20Hz), we can down-sample, as shown in Fig. 4.6. In this case, even if only every third sample is used by the dynamic model at a given instant, the prior Gaussian smoothing incorporates a significantly larger temporal window into this data. Note that the 20 Hz model is still *updated* at 60 Hz, but it models dynamics below 10 Hz while ignoring higher frequencies in the input signal.

Finally, the output command from the brain will drive a visual feedback signal. As mentioned previously, 30 Hz is at the lower end of refresh rates used for computer games, and should be a reasonable rate for this application. Most computer displays now support a refresh rate of 60 Hz or above. In the absence of other hardware constraints on computation, there is no reason not to implement the system at a base sampling rate of 60 Hz. Thus, a model implementation allowing a small number of parameters to capture desired low-bandwidth dynamics can be implemented in a digital system with a high sampling rate for smooth and responsive visual feedback.

4.7 Conclusion

We have described three areas for improvement in BCI systems which can be implemented without significant additional computational requirements or changes to the underlying models used to decode brain activity: (1) Gaussian kernel smoothing using a kernel width optimized for observed cell behavior provides the best firing rate estimate with the lowest latency among other choices of smoothing filters; (2) careful choice of dynamic model structure and number of parameters can improve the performance of decoding algorithms, potentially leading to improved performance of decoder-based BCIs; and (3) implementing the full system at a sampling rate of 60 Hz will allow faithful reproduction of the underlying continuous-time dynamics and provide seamless and smooth visual feedback to the subject. Together, these improvements should facilitate substantial performance improvement of existing BCI designs.

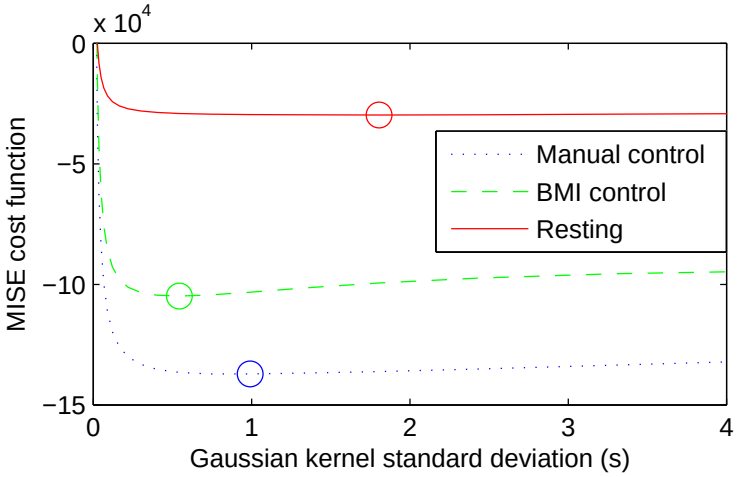

Figure 4.3: Estimated MISE as a function of Gaussian kernel bandwidth for the same neuron in different recording conditions. Optimal bandwidths, marked by open circles, are different, but in relatively flat regions of the cost function. Sample data sets are 1- to 3-minute single neuron recordings from microwire array in motor cortex of a macaque monkey.

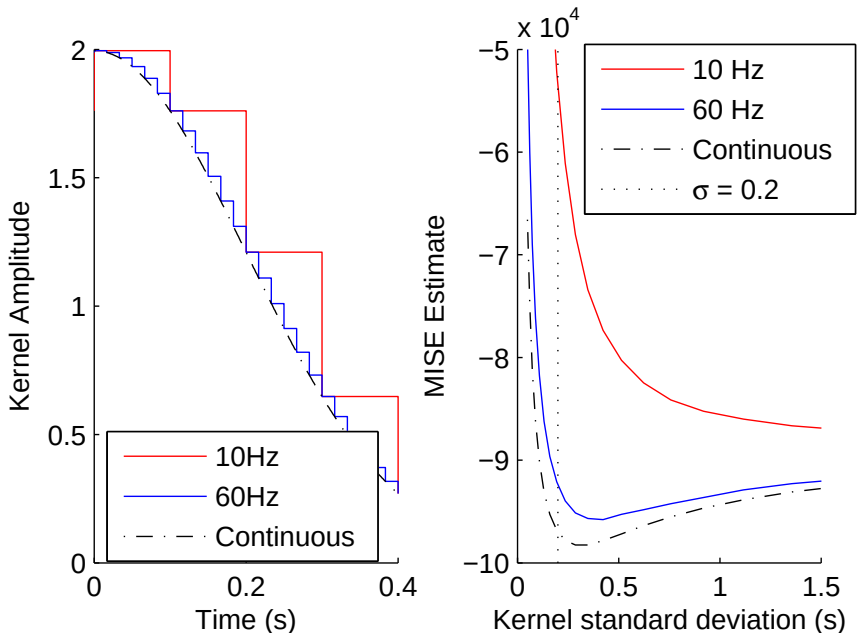

Figure 4.4: Comparison of continuous and sampled Gaussian kernels, $\sigma = \mathbf{0.2s}$, at left, and MISE cost as a function of standard deviation at right. Sampling rate affects both the minimum achievable MISE and the optimal bandwidth to achieve minimum MISE. Note that this analysis does not account for the latency in the firing rate estimate introduced by the use of a causal filter. Sample data recorded from motor cortex of macaque during 10-minute brain control session.

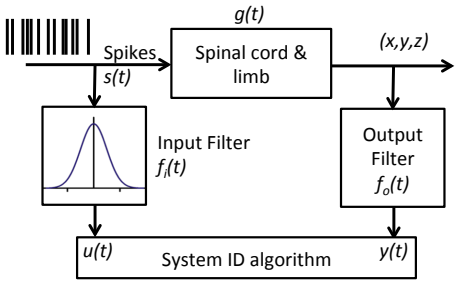

Figure 4.5: Block diagram illustrating the system identification problem for decoding limb movement. The relationship between $u(t)$ and $y(t)$ is only equivalent to the spinal cord and limb transformation if the output filter is the same as the input smoothing filter.

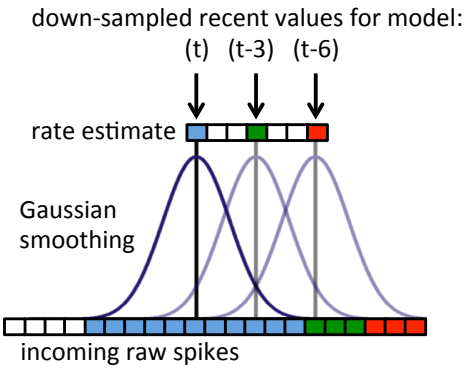

Figure 4.6: Illustration of down-sampling spike rate estimate to increase temporal window of data available to model while decreasing redundancy of sample information. The transparent Gaussian kernels and green and red samples represent delayed copies of the current filter output (blue) used by the model.

Chapter 5

CONTROL POLICIES EVIDENT DURING BRAIN-COMPUTER INTERFACE TASKS

5.1 Chapter Summary

Brain-computer interfaces (BCIs) translate user intentions into real-time commands for closed-loop control. This is done by decoding intention from neural activity, such as recorded single-unit spiking. Studies have successfully shown decoding of not only instantaneous movement parameters, but also of anticipated movement information and of movement endpoint goals. This has been leveraged to use predicted movement intention as a BCI command, improving performance in a closed-loop paradigm with significant delay in the forward pathway. However, BCI performance is also attributable to adaptation by the brain. Optimization of closed-loop BCI performance is an instance of the *dual control* problem, wherein control and estimation are not separable into independent design problems. Consequently, it depends critically on knowledge of the control policy chosen by the brain. An interesting question is whether the brain chooses to utilize past and predicted movement information in determining instantaneous BCI commands. Reasons for doing so include compensation for forward pathway latency and for sensory processing delay. It has already been shown that BCI commands are accounted for by forward task state prediction from delayed sensory information. Here, we show that control based on past, immediate, and predicted task state is demonstrated during manual control of a novel force-modulation task. We then show that a similar policy is applied to the modulation of single cortical units during BCI control of an analogous task.

5.2 Introduction

Intracortical brain-computer interfaces (BCIs) make use of decoding algorithms mapping high-dimensional neural activity to a low-dimensional command signal. Their development

has been driven by two pivotal discoveries: that the brain is capable of modulating single-unit activity if provided appropriate closed-loop feedback [19, 20], and that tuning functions can often at least partially explain the relationship between single-unit activity in motor cortex and movement [26].

Many BCI architectures are based on tuning functions, which correlate cortical activity with limb kinematics or to more abstract task variables, such as computer cursor position. The latter have the advantage of being well-defined during brain control or observation of task performance. Such BCIs [30, 10, 27, 70] estimate instantaneous movement intention by assuming that neural firing rates are linear functions of movement state variables. By using decoded intention as a command, BCIs create an unfamiliar control loop.

The use of a neural decoder of movement state information as a BCI command source imposes a change from *estimated* or *observed* movement to *intended* movement upon the encoded latent variables. Consequently, the tuning functions relating neural activity to task variables constitute a control policy, which in turn determines closed-loop performance of a BCI system. This motivates our analysis of neural modulation during BCI tasks explicitly as a control policy, and in comparison to force modulation during manual tasks. It should be possible to identify the control policy which determines muscle activation based on task state, assuming muscle activation is not predominantly pre-planned. These control policies determine the performance, stability, and robustness to disturbances of motor control during movement.

5.3 Background

In this section, we discuss the control problems faced by the brain, before reviewing previous findings about how the brain performs state estimation, and what assumptions are made about the brain's control strategy to co-adapt BCI decoders.

5.3.1 Framing the Control Problem

Because neural computation and transmission in both afferent sensory pathways and efferent motor control take time, latency tradeoffs exist in the choice of control law. Given the delay for sensory information to reach cortex, the CNS can either control based on delayed state

information, or predict ahead by some time interval at the cost of estimation uncertainty. This also means that estimating immediate task state from delayed sensory information is an integral part of control. BCI commands have been shown to be consistent with control based on cursor position estimates predicted from delayed visual information [29].

Automatic control systems, such as those in robotic manipulators or aircraft autopilots, encounter similar challenges in the timing of information availability. An important function of Kalman filters and other state estimators is to provide a continuously updated state estimate despite intermittent and possibly delayed measurements. Sensing and actuation involve delay of dynamics as well as transmission, and techniques for mitigating the consequences of these on performance include controlling based on accurate but delayed state information, as well as predicted but uncertain state.

Feedback based on delayed sensory information avoids the prediction inaccuracy of a state estimator, while controlling based on predicted error may help compensate for latency in the neuromuscular system. Controlling based on current task state necessarily involves prediction uncertainty and suffers the performance consequences of delay in neuromuscular dynamics. A reasonable question to ask is: Do motor control policies act directly upon delayed or predicted state information, as well as upon current estimates? These tradeoffs, and their differences between manual and BCI-mediated control, are illustrated in Figure 5.2.

5.3.2 Prior Work Identifying State Estimation in Cortex

We highlight two studies which have provided the most detailed knowledge of state estimation performed by the brain during BCI-mediated control. One study shows that predictably incorrect control actions are generated when the BCI decoder is replaced with a perturbed version [29], without invoking a specific state estimator model. A more recent study derives a linear-Gaussian internal model estimation framework which supports the hypothesis that errors during BCI control are attributable to an incorrect internal predictive model in combination with sensory processing delay [28]. Note that studies treating the BCI as an estimator of brain state, such as [27, 30], equate task control input $\mathbf{u}(t)$ with brain state es-

timate $\hat{\mathbf{x}}(t)$. This should not be confused with the brain's internal state estimator: the $\mathbf{u}(t)$ decoded (but not used) during manual task performance or task observation is an external estimate of the brain's estimate of task state.

5.3.3 Control Policy Assumptions in BCI Co-Adaptation

To date, limited assumptions have been made where there is a need to know what control policy is applied during BCI control. Frequently, these entail assumptions about direction, but not magnitude, of a 2D BCI command. The challenge of not knowing the subject's movement intentions during BCI-mediated control, and that they may differ from those during manual control, is well-recognized [27]. In [16], for example, experimenters perform decoder adaptation "based on the assumption that the monkey intends to move to the target at all times and intends to cease moving when hold on the target to select it." However, experimental results unambiguously contradict this assumption, as noted in [28]: "It is an open question as to why the subject does not always drive the cursor straight to the target." Thus, identifying the control policy used by the subject has the potentially to greatly improve the process of fitting adaptive decoders against experimental data.

5.4 Methods

5.4.1 Electrophysiology

A macaque is implanted with dual 96-channel microelectrode arrays (Blackrock Microsystems, Salt Lake City, UT), bilaterally in motor cortex, connected to a 128-channel Cerebus neural signal processor (Blackrock). Manually set time-voltage criteria are used for online spike sorting, which is recorded at 30KHz for offline analysis. Custom LabVIEW software (National Instruments) is used to implement the BCI decoding algorithm and behavioral tasks. We conduct experiments in a primate behavior booth outfitted with a computer monitor, buzzers, and a computer-controlled feeder containing apple sauce. The animal's arm, contralateral to the implanted array, is situated in a custom 2-DOF near-isometric manipulandum. The computer monitor is 30 cm x 23 cm, located 28 cm in front of the animal's head. The decoding algorithm and cursor task operate at a sampling rate of 60Hz,

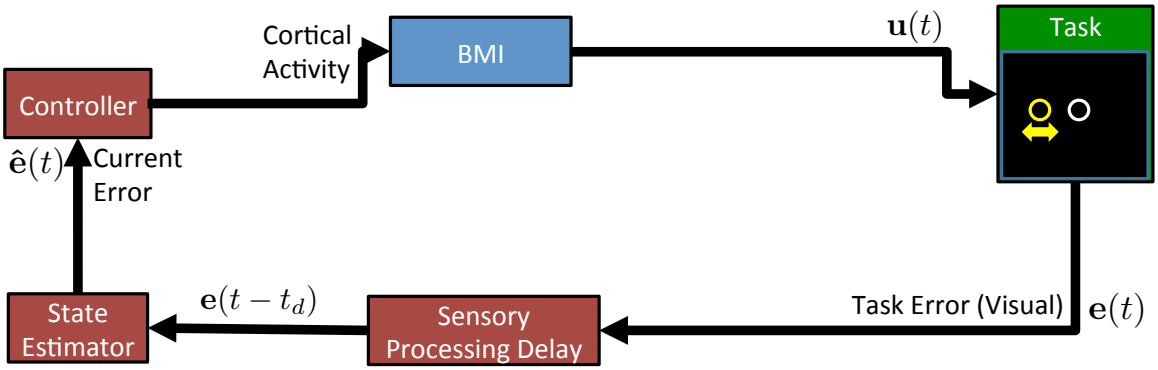

Figure 5.1: The hypothesized BCI control system architecture supported by the experimental work of Golub et al [29, 28]. Red blocks indicate processes internal to the subject, while blue indicates external interface components. Visual processing latency of t_d is compensated for by the use of an internal state estimator to generate estimated task error state $\hat{\mathbf{e}}(t)$. The specific algorithm used for state estimation is unknown, but experimental results are consistent with a linear-Gaussian process. The form of the controller is unknown, but its output is believed (and forced, by consequence of system design) to encode current intended movement derived from internal estimates of current task state.

with the target display refresh rate 30Hz. The BCI system input-output latency is measured to be about 50ms.

The manipulandum is used for task training and to measure neural correlates of motor activity. This eliminates the possibility that neural activity is accounted for by tuning functions to limb kinematics or dynamics, since there are minimal postural changes.

5.4.2 BCI Architecture

We implement a simple decoder based on population vector mapping [26]. For each unit, spike counts in 16.7ms bins are first filtered with a truncated Gaussian kernel, $\sigma = 0.05s$, before a baseline firing rate estimate is subtracted and the resultant instantaneous modulation estimate contributes to the population vector sum $\mathbf{u}[t]$ according to

$$\mathbf{u}[t] = \mathbf{u}[t-1] + \sum_{i=1}^{N} \alpha_i (f_i[t] - \hat{b}_i[t]) \tag{5.1}$$

$$\hat{b}_i[t] = \hat{b}_i[t-1](1-\gamma) + f_i[t]\gamma \tag{5.2}$$

where the baseline rate $\hat{b}_i[t]$ for each filtered firing rate $f_i[t]$ is continuously updated using an exponential moving average filter with decay constant γ. Modulation from each of N cells, typically $N = 4$, are summed with weights $\alpha_i = \pm 0.01$. The same algorithm is used to implement manual control tasks, where $f_i[t]$ is replaced with a torque signal and the sum is assigned to $\mathbf{y}[t]$ for direct position control.

5.4.3 Behavioral Tasks

We present the macaque with two different 1D cursor position control tasks: during manual control (MC), isometric wrist torque determines cursor velocity, and during brain control (BC), velocity is determined by aggregate cortical single-unit activity via Equation 5.2.

For a successful trial, the cursor center must be held within the target radius for 1s. Targets appear randomly, and a 1/2 second break is provided between trials. Cortical units and the direction of their mapping in the decoder are often, but not always, selected on the basis of observed correlations with torque production during manual control. During brain control tasks, wrist torque is still recorded for later analysis, although it has no direct effect on the cursor task. We can augment the block diagram in Figure 5.1 to capture both manual and brain control, as shown in Figure 5.3 with the new blocks highlighted in yellow.

5.5 Modeling Control Policies

Several steps are involved in identifying linear models capturing control policies. First, we need to classify the input-output data sets we believe capture exactly and only the relevant control policies. There are two components of this selection process: 1) choosing which time-domain data to include in a single data set, for consistency with the assumption that it is captured by a single model and parameter set, and 2) determining the bandwidth of the identified system.

5.5.1 Grouping and Pruning Trials

To address the first question, we first group trials into continuous experimental blocks, and then only examine data during the corrective feedback portions of each trial. This is to exclude initial, possibly pre-planned, movement, as well as inter-trial waiting periods. We need to avoid fitting to control actions that are dominated by pre-planned, or open-loop, control. To do this, we fit only the portion of each trial *after peak velocity*, assuming that corrective control dominates this portion, as illustrated by the example trajectories in Figure 5.4. To address the second question, we can do a spectral analysis of our data and consider our assumptions about information coding in neural activity.

5.5.2 Pre-Processing for System Identification

Before a model of neural modulation can be fit, instantaneous firing rates must be estimated from recorded spike trains. The commonly-used histogram method for estimating instantaneous rates involves counting the spike events within non-overlapping time windows, or bins, of some size. A frequently used bin width is 100ms [3, 55, 50], with precedents [69, 68]. The Gaussian filter has been shown to out-perform the histogram method [53] for offline firing rate estimation. We use a Gaussian filter designed to capture neural modulation below a cutoff frequency, which separates rate-coded information from Poisson process variability treated as noise (see Chapter 4).

Spectral analysis of cursor trajectories during manual control indicate that on average, 95% of signal energy in velocity-control tasks is below 4.3Hz, and 3.5Hz in position-control tasks. This is consistent with the bandwidth observed in a similar experiment [68]. Since linear models can only capture dynamics falling within both the input and output bandwidths, we choose a Gaussian filter bandwidth to admit the (lower bandwidth) torque signals [42]. We use a Gaussian kernel with a standard deviation of 30ms, resulting in a 4.4Hz corner frequency and -20dB attenuation at 11.5Hz. We then restrict our analysis of single units to those with a mean firing rate above 15Hz, to avoid modulated firing rates at frequencies not well-attenuated by the Gaussian filter; 4.4Hz can be considered a lower bound on the firing rates captured by the filter and linear model. When fitting a model to neural signals,

we filter both input and output (e.g. task variables and firing rates, respectively) with the same filter [42].

When fitting a model to the relationship between torque and task error, we do not filter, assuming insignificant high-frequency noise in the torque signal as limited by the physical dynamics.

5.5.3 Modeling Approach

Our modeling approach is based on an initial hypotheses that control is proportional to cursor position error, and to the rate of change of this error (Figure 5.5). In control theory literature, this is known as proportional-derivative (PD) control [44], and it can be thought of as equivalent to neural tuning of position and velocity (relative to target), commonly used in BCI decoders. However, we are particularly interested in any time offset between control actions and state information, so we search a space of time offsets for the best descriptive power of observed control. This process produces evidence of control based on substantially delayed and predicted task state, which in turn motivates a change to the model structure and re-fitting with the more complex model. The complete model (Figure 5.7) includes control proportional to delayed and predicted task error, in addition to PD control based on current task state.

We begin with the approximation that feedback control strategies are captured by linear functions of current task state, which includes PD control. There are multiple ways to implement PD control with a discrete-time system representation; in Figure 5.5, we show how a pair of impulses can do so. By using impulses with variable time offsets as the basic component of our model, we can easily capture control policies based on delayed or predicted state, and use a parsimonious yet expandable model structure.

We use a discrete-time model which allows linear feedback of time-shifted state. Sparse sampling of the input signal reduces the number of parameters while maintaining high descriptive power, similar to autoregressive models used for decoding limb movement [21]. The control signal $\mathbf{u}[t]$ is driven by cursor state $\mathbf{e}[t]$ in error coordinates according to

$$\mathbf{u}[t] = b + \sum_{i=1}^{n} a_i \mathbf{e}[t + \tau_i] + \epsilon[t] \tag{5.3}$$

where control signal $\mathbf{u}[t]$ may correspond to wrist torque, single cortical unit firing rate, or to the population vector sum of firing rates (BCI ensemble modulation). Input sample weights a_i are paired with time offsets τ_i, which are not necessarily sequential. A torque offset during manual control, or baseline firing rate of cortical units, is captured by b. Linear regression is used to choose the sample weights a_i and offset b, and optimization is used to choose the time offsets τ_i resulting in the best goodness-of-fit. Residual errors are represented by $\epsilon(t)$.

Because we define the model input $\mathbf{e}[t]$ to be cursor position only, cursor velocity is not provided directly, but the model parameters can be chosen to implement a derivative approximation. Of multiple imperfect discrete-time approximations of the derivative, the difference of two sequential samples is the simplest. Therefore, we initally set $n = 2$, permitting the model to implement a PD controller or to use only proportional control at two different time offsets. We will increase the number of model samples n as justified by significantly improved descriptive power, and as consistent with our hypotheses about additional delayed and predicted control terms.

5.5.4 Model Selection

Figure 5.6 shows an example of model goodness-of-fit as a function of the two time offset parameters τ_i for one 10-minute block of manual velocity-controlled trials. We find local maxima at a point that effectively implements a PD controller (2 samples with 1 sample period of separation) based on current state, and additionally at a point combining future and past task states.

That we do not see 4 maxima suggests that the pair of samples constituting the PD controller has substantial dependence on the sequential difference for explanatory power. This is lost if one of those samples is replaced with a significantly time-shifted sample. For example, given maxima at offsets of $(0, \tau_\epsilon)$ and (τ_d, τ_p), if the first pair's explanatory power did not come from the difference operator, we could expect maxima at $(0, \tau_p)$ and (τ_d, τ_ϵ).

Based on this preliminary modeling, we hypothesize that predicted and delayed state are also used for control, resulting in the closed-loop architecture shown in Figure 5.7. We therefore apply an $n = 4$ model and test the constraint that two of the samples must have

time offsets within the range $[-5, 5]$, for consistency with the hyothesis that a PD controller exists. Our search domain for these samples extends to $[-10, 10]$, allowing the model to fail entirely if the data is inconsistent with PD control. We additionally constrain the other two samples to have offsets with opposite signs and maximum values of 60 samples (1s). We use these parameter restrictions and model rejection criteria because without them, in some cases the optimization process returns time shifts and and gain values consistent with a PD controller implementation utilizing either the delayed or predicted term, which is inconsistent with our hypotheses. Five samples corresponds to about 83ms; if one of the intended PD terms has a greater time shift than this, there is ambiguity about whether the term is better considered a predictive or delayed term.

The additional two terms further improve goodness of fit, supporting our hypothesis; later, we will use F-tests to confirm that this improvement is significant. We will proceed using the $n = 4$ model, identifying the control strategies used during brain and manual control for all of our data sets, and rigorously testing the significance of the additional model terms.

In contexts where our model has good descriptive power, we will support the hypotheses that the control policy entails PD control in addition to predictive and delayed terms; our goal is to establish that this is the case for torque modulation during manual tasks, and for neural modulation during BCI-mediated tasks. We are not concerned with the specific values of the gain parameters identified for each data set, and do not need them to be similar to support our hypothesized control architecture. Good model predictive power under the constraints we impose on the time offsets is sufficient to support our hypothesized architecture, and we will compare time offsets between manual and BCI-mediated control to identify any subtle differences.

5.6 Results

We fit the constrained $n = 4$ model architecture to torque feedback and to neural modulation during both BCI and manual control. Our hypotheses are supported if the same model structure not only describes manual control strategies, but also neural modulation strategies during BCI control. Table 5.1 summarizes the consistency of our data with increasingly

detailed model assumptions, for all of the relationships we expect it to describe: torque modulation in response to position error during manual tasks, and single-unit as well as population vector ensemble modulation in response to position error during BCI-mediated tasks.

Additionally, we would like to see the model fail to describe signals we did not hypothesize to be part of a control policy. We can improve support for our hypotheses by showing that its descriptive power is unique to our hypothesized control system input-output relationships. This will provide a negative control for the model's descriptive power. We therefore apply the same model to manual *effort* during brain control, and to neural modulation during both manual and brain control. In all cases, task state (cursor position error) is the input variable for the model. Aggregate modeling results, in terms of goodness-of-fit, are shown in Figure 5.9.

Goodness of fit is consistently very high for describing torque modulation during manual control. Neural modulation is very poorly predicted by this model structure during manual control, but predictive power improves during brain control - whereas predictive power of manual effort decreases during brain control. This supports our hypothesis that the brain may apply a similar control strategy as is evident in manual control, including the use of predicted and delayed control terms, to the novel cortical interface provided by the BCI.

Next, we examine the aggregate results for identified time shifts of the delayed and predicted model terms. As shown in Figure 5.10, we do not see a significant change in the delay interval or in the prediction interval when comparing manual to BCI-mediated control. The distributions of time offsets of the PD shifts have slightly positive median values ($\leq$ 1sample) in both cases, suggesting that the PD control entails a slight prediction interval. What is most remarkable about the time shift estimates between manual and BCI-mediated control is the lack of significant change, despite substantial changes in the sensory processing delay and forward path latency.

5.7 Discussion

We began by modeling BCI and manual control with a simple PD model, which unsurprisingly provided modest descrptive power. We then, to our knowledge for the first time,

showed that BCI-mediated task control strategies also utilize time-delayed and predicted task error state. Specifically, these components provide significant additional explanatory power compared to PD control strategies alone. That the brain does this is highly relevant to the closed-loop design of BCIs, and in particular suggests that redundancy may exist if a BCI attempts to compensate for processing delays or robotic manipulator dynamics, such as in [70]. Finally, we examined the time shifts of the different control policy components, and our results suggest that the brain may not be able to adapt to novel interface paradigms whose timing properties lay outside that of the native motor system.

To date, a central component, and challenge, of implementing high-performing BCIs is correlating intended commands with decoded commands. This information is used to initialize decoder parameters, and more importantly to co-adapt decoders. Fundamentally, it is the data needed by neural engineers to build a basic understanding of how cortex is involved in movement control. One aspect of this that is particularly salient for BCI design is the question of causality: which signals in cortex reflect observation and perception, and which reflect intention and planning?

We must also point out that the use state of estimators, in particular Kalman filters with second- or third-order dynamic models of cursor or limb movement, impose assumptions about the dynamics of command signal evolution. Contrast the dynamic response of a system under control (e.g. a person on a bike) with the dynamic response of a servo controller (e.g. arms on handlebars) able to deliver rapid settling time and excellent disturbance rejection: the controller has much faster dynamics than the plant. Yet, current BCI designs impose an assumption that controller dynamics are equal to that of the plant. These assumptions may currently serve the purpose of filtering noise, but they will ultimately severely limit performance.

Our work here represents a modest but important step towards developing better predictive models of how the brain controls movement, which represents fundamental knowledge as well as an enabling tool for improved BCIs. Great benefit may be derived from future work investigating the range of variation exhibited by cortical control policies, and any systematic rules explaining adaptation based on BCI decoder properties and closed-loop dynamics.

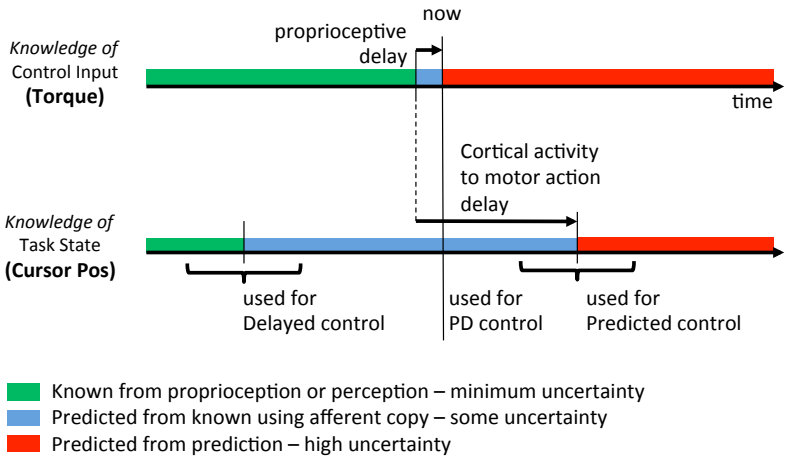

(a) Manual Control

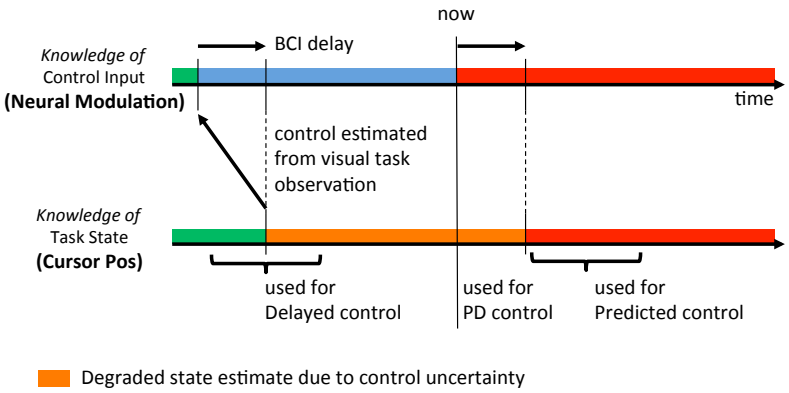

(b) Brain Control

Figure 5.2: Timing diagrams showing the quality of information, available in cortex, about executed control actions (top lines) and about task state (bottom lines). Timing for manual task control (5.2a) and during BCI-mediated control (5.2b) are different. Direct perceptions of control and of task state are delayed by afferent feedback latency and visual processing latency, respectively. Consequently, control actions dependent on immediate state must use predictive estimates. During brain control, afferent feedback of control is unavailable or highly uncertain, so it must be estimated from task state. This degrades the quality of immediate state estimates available for control decisions, and could prompt a shift in control strategy. We test for changes in the time shifts of delayed and predictive control.

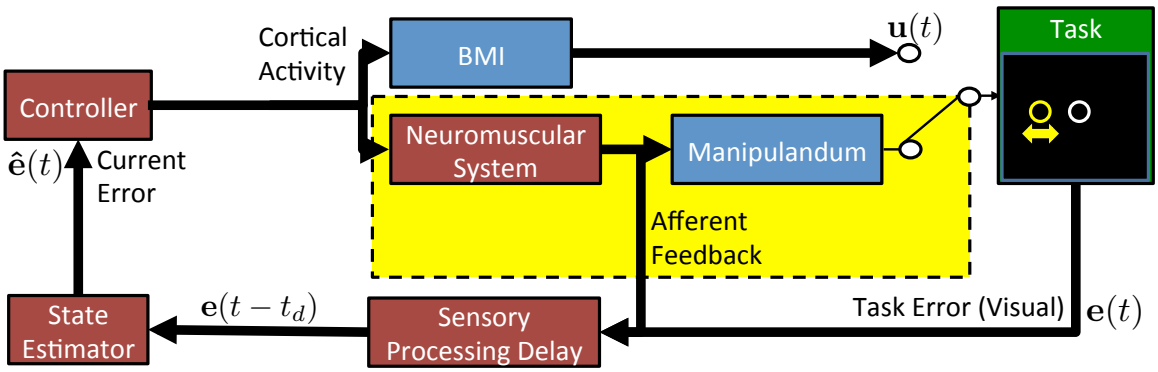

Figure 5.3: BCI control system architecture augmented with an alternate pathway capturing manual task control, with new blocks inside the highlighted region. Task conditions are repeated in both BCI-mediated and manual control for comparison. Afferent feedback from the limb may provide lower-latency information about the generated control input to the task, but not directly about task error state. We do not attempt to prevent the erroneous use of torque and afferent feedback during BCI-mediated tasks. Instead, we test whether torque modulation is still described by our control policy model even though it has no direct effect on the task.

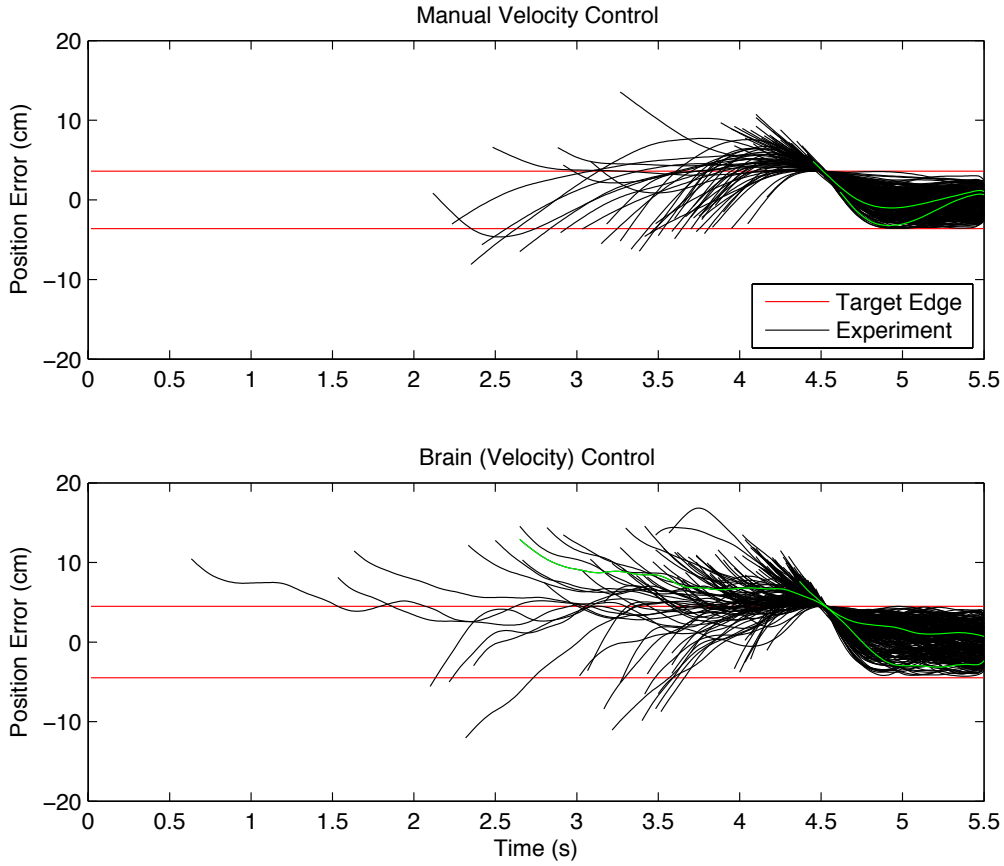

Figure 5.4: *Top*, successful task trajectories from a 10-minute trial block of manual control of cursor velocity. *Bottom*, BCI-mediated control of cursor velocity. The vertical axis is cursor position relative to target, and the horizontal axis is time. All trials are aligned to have the same *end* time, so all trajectories enter and remain within the target bounds 1s before the end. To simplify visual display, position error is negated for some trials so that all trajectories' final target approaches are from the same side. Trajectories are truncated prior to the time of maximum velocity within each trial, in order to capture corrective control actions rather than feed-forward or pre-planned control actions.

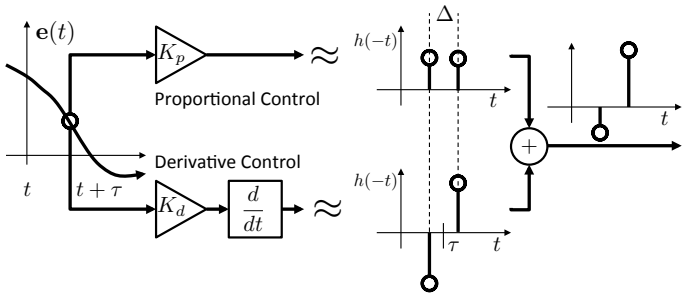

(a)

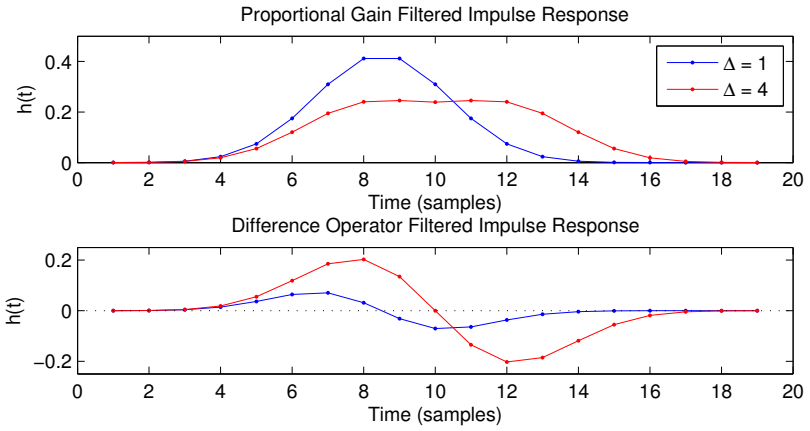

(b)

Figure 5.5: (a), Illustration of two-term impulse response functions to implement proportional-derivative control policies in discrete time. We begin by sampling an error signal $\mathbf{e}(t)$ with time offset τ and calculating proportional and derivative control terms from this error. Since τ is positive, the use of a predictive state estimator is implied but not shown here. Proportional control can be accomplished by a single time-shifted impulse, corresponding to an (α_i, τ_i) pair in Equation 5.3. The addition of a second impulse has little effect if the time separation Δ is short. Next, the difference operator is an approximation of the derivative, and equivalent to sequential impulses of equal and opposite magnitude. Thus, an impulse response function of two terms with short time separation can implement a proportional-derivative control policy. Or, an isolated impulse is equivalent to time-shifted proportional control. The impulse responses of each control type in combination with our low-pass Gaussian filter is shown in 5.5b, showing that for Δ up to at least 4, the filters are functionally similar.

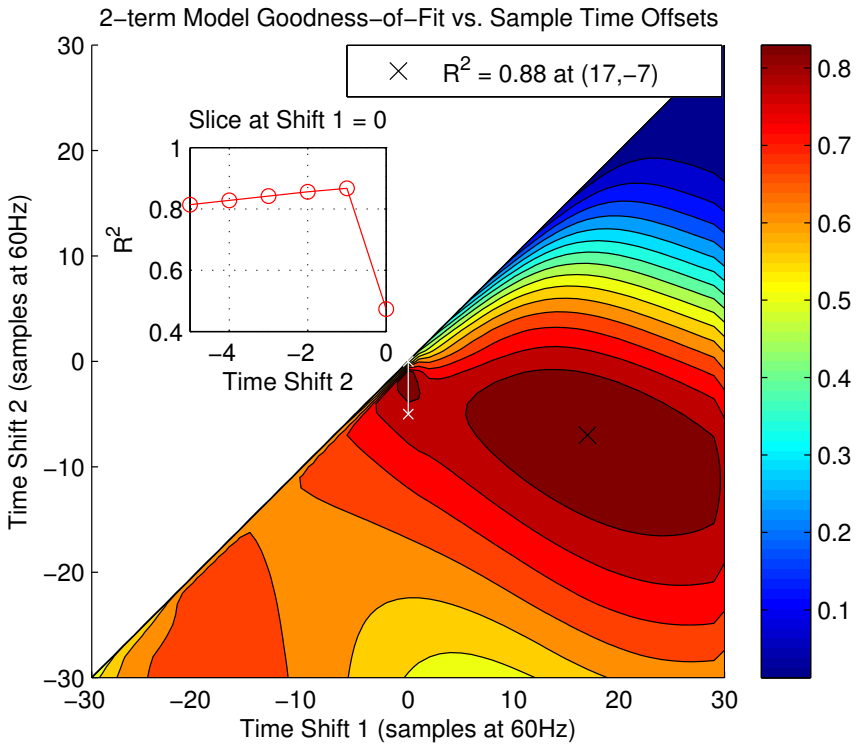

Figure 5.6: Goodness-of-fit of a two-term model of torque response to cursor position error, as a function of the time shift of each control term. The upper triangle of the domain is not shown because it is symmetric with the lower triangle, and goodness-of-fit along the diagonal is equal to that of a single-term model since the time shifts are equal. The surface has a local maximum near the origin (along the white line) consistent with PD control, and an unexpected global maximum, marked with black $\times$, combining future and past state values. Detail of the local maximum consistent with PD control, a time shifts $(-1, 0)$ samples, is shown in the inset. The absence of a local maxima at one time offset from the PD pair and one from the significantly shifted pair is consistent with the hypothesis that the nearly-sequential samples implement a PD controller. A greedy approach to identifying a controller model dictates choosing the global maximum, whereas imposing the assumption of PD control motivates choosing the maximum near the origin. In either case, identification of additional control terms is warranted.

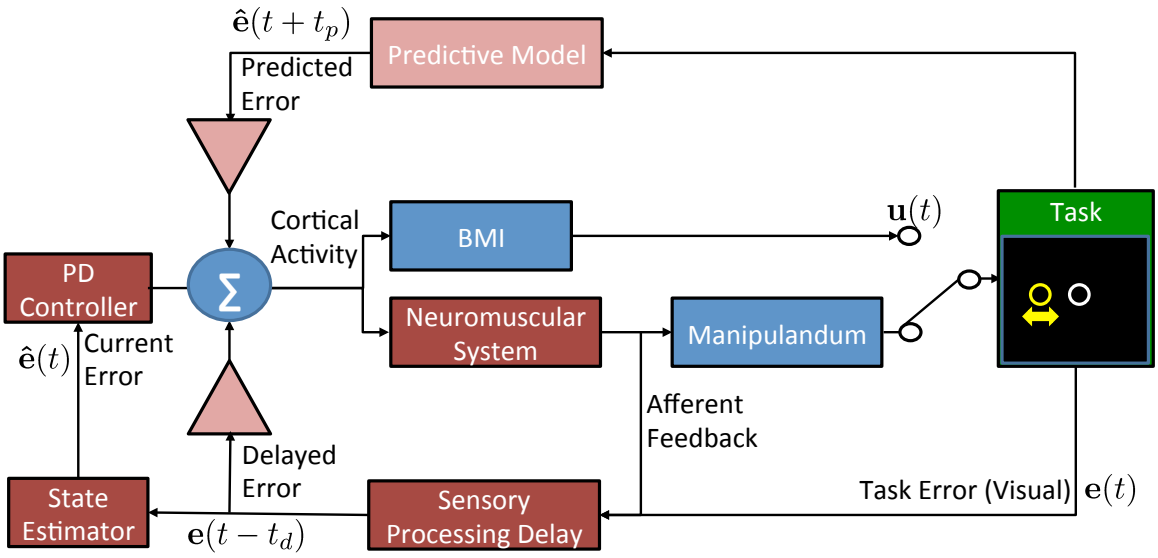

Figure 5.7: Hypothesized neural control architecture with added blocks (light red) to capture control actions proportional to delayed and predicted task error, summed with PD control. These changes are motivated by the global maximum in Figure 5.6. The predictive model is unknown, and we substitute ground-truth future task state for this estimate for model identification, just as actual immediate task state $\mathbf{e}(t)$ is substituted for estimated immediate task state $\hat{\mathbf{e}}(t)$.

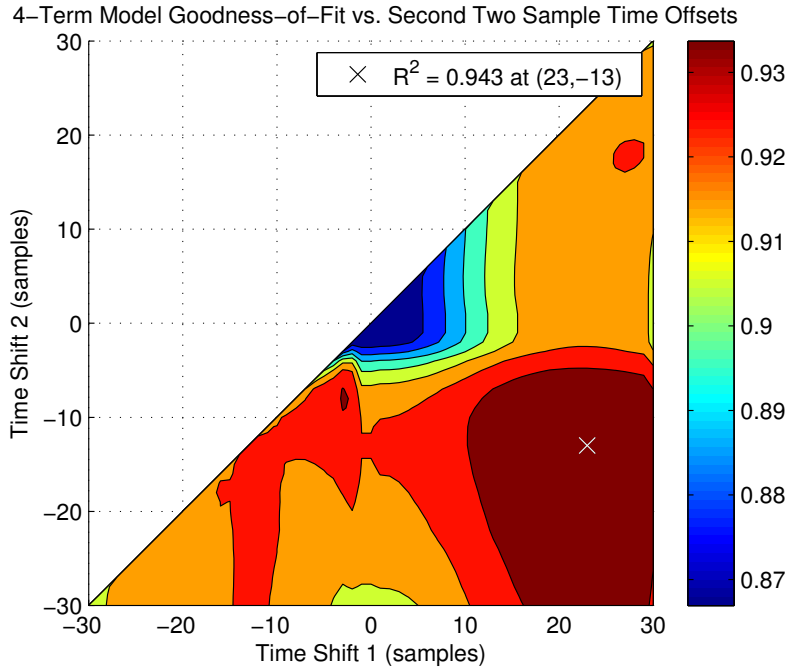

Figure 5.8: Goodness-of-fit of a four-term model of torque response to cursor position error, as a function of only the *second two* terms' time shift. Consequently, the minimum performance is equal to the global maximum from Figure 5.6, and occurs near the origin where the second two terms are most redundant with the first two terms. A global maximum exists that is consistent with delayed and predictive control terms in addition to the PD control terms in the model. Thus, a controller model has been identified that is consistent with PD control in addition to control proportional to delayed and predicted task state.

Condition	Torque/Manual	Single Units/BCI	Ensemble/BCI
Total Trial Blocks	58	270	69
% Consistent with PD control	100%	96%	99%
% Consistent with PD + Predictive	100%	96%	99%
% Consistent with PD + Delayed	71%	93%	94%
% Consistent PD + Predictive + Delayed	71%	93%	94%

Table 5.1: Assessment of model parameter consistency with architecture assumptions. From the top to the bottom rows of percentages, increasingly detailed criteria are applied to identified model parameters for each trial block, to determine whether they are consistent with the hypothesized control architecture in the left column. The PD pair of terms had to have opposite signs and a time separation of at most 4 samples, while the parameter optimization was only constrained to keeping each term of the PD pair within ± 10 samples but discarded results outside of ± 5. Further, the predictive and delayed terms had to have time shifts of appropriate sign. The majority of models in all cases had parameters consistent with the architecture assumptions. Additionally, we performed F-tests on each four-term model against each of the three simpler model types, using the same time offsets as applicable. More than 95% of trial blocks passed these F-tests in each task condition, confirming that the four-term model is significantly better.

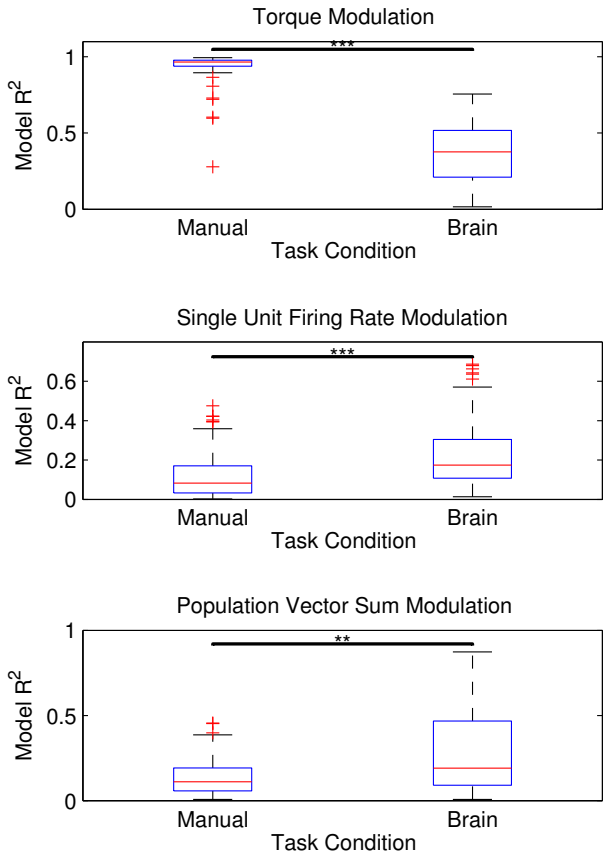

Figure 5.9: Goodness-of-fit of four-term models to neural and torque modulation between task conditions. Top, the median R^2 value for modeling torque modulation as a function of task error is 0.966. This descriptive power is diminished significantly ($p \leq 0.001$) during brain control compared to manual control, suggesting that the subject has abandoned a manual control strategy. Conversely, descriptive power of neural modulation increases significantly during brain control compared to manual control: the median R^2 value rises to 0.174 ($p \leq 0.001$) for single units (center panel), and to 0.191 ($p \leq 0.01$) for the BCI control signal determined by ensemble modulation (bottom panel). For inclusion in this analysis, model parameters for each trial block had to include a pair of terms with opposite sign and at most 4 samples of time separation, consistent with PD control, and the remaining two terms had to have time shifts of opposite sign.

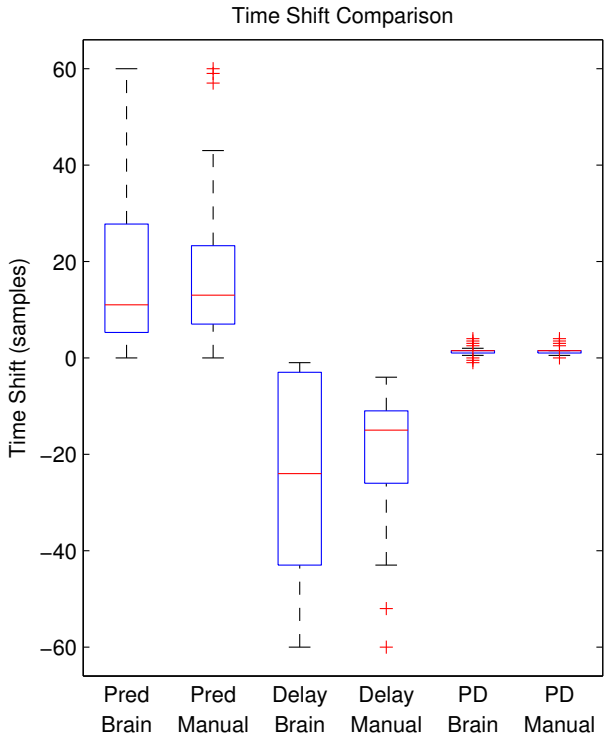

Figure 5.10: Distributions of identified time shifts of control terms between task conditions. Modulation of single units is analyzed during brain control, and torque modulation is analyzed during manual control. Control terms and consequently time shifts are categorized as part of the PD pair, a proportional delayed term, or a proportional predicted term. No significant differences are shown by our results, which include 64 trial blocks of single units and 30 trial blocks of manual control. This suggests that the subject does not respond to the increased perception latency and estimate uncertainty with changes to the time shifts of delayed and predictive control terms.

Chapter 6

CONCLUSION AND FUTURE WORK

This thesis has provided a valuable performance metric for the evaluation of BCI systems, new insights about performance tradeoffs in pointing interfaces, and new knowledge of the strategies employed by the brain during BCI control. Here we summarize these findings, and discuss the doors they open for further investigation.

We have shown the Shannon-Welford model of aimed reaching movements to provide better explanatory power of the duration of BCI-controlled 1D movements than the incumbent Fitts's law. It can be used to compare between studies, provided that researchers publish the physical units of movement scale and the range of geometries tested in experiments.

Our use of a logarithmic transform to accomodate log-normal movement time distributions enabled the adaption of this performance metric. We hypothesize, but have not shown, that this distribution is attributable to the *dwell-to-select* task behavior. It would be interesting to investigate whether this distribution arises with interfaces familiar to the user, but incorporating the dwell-to-select feature. A more practical direction of future work for BCIs may be the investigation of crossing tasks for 2D interfaces, which have previously been shown to follow Fitts's law [1]. The use of crossing tasks would eliminate the extra parameter of experimenter-chosen dwell time when comparing across studies.

We have used the Shannon-Welford model's movement time prediction surfaces to provide insight into performance tradeoffs across a wide range of task geometries. In particular, the $k = 1$ condition may represent a performance-maximizing gain choice across the widest range of geometries. The choice of geometries can shift the performance-maximizing gain, in extreme cases from the largest tested to the smallest tested. Aggregating user-reported ease-of-use across multiple studies suggests that performance/effort tradeoff may be optimized at or below $k = 1$, although we do not know what all cost factors contribute to ease-of-use. The slope of the gain vs. k line is affected by interface stiffness, suggesting that

scale of proprioceptive feedback may be a contributing factor.

Our results correlating performance-maximizing properties with the value of k are important and useful because they permit comparison across entirely different interface modalities, where gain itself cannot meaningfully be compared, such as in [49]. Specifically, we assert that gain selection should be considered a confounding parameter if it is not selected to achieve the same k value when comparing across interfaces.

The variable gain analysis results leave several open questions for future work. First, what will the gain vs. k line look like for an interface that provides little or no proprioceptive feedback, such as myocontrol? Our results suggest it would be extremely steep. Second, what will reported ease-of-use as a function of k look like? With myocontrol, increased contraction will add noise instead of increasing limb stiffness, so additional effort will only improve performance if it is used to produce larger accelerations. Will the brain realize a controller matched to this context? What will reported ease-of-use vs. k be for an interface that does not incur a significant metabolic cost of operation at all, such as a BCI? Again, will the brain realize an optimal strategy in this context, or make marginal adjustments to the control policy used for native limb movement?

Another interesting tangent from the CD gain work is an investigation of how visual task scale is defined by the brain. We have not made a distinction between display scaling measured as physical size vs. as visual angle; experimental manipulations could uncover separate affects of these two factors.

Finally, we showed that a simple controller accounts for both novel manual control and BCI control of velocity. To our surprise, it incorporates predictive and delayed feedback terms. The incorporation of predictive and delayed terms motivates design of closed-loop BCI systems utilizing this new model. Future work with 2D interfaces can establish whether the architecture we identified here also explains the angle of commanded velocity during BCI-mediated tasks, a phenomenon of persistent mystery [28].

The most surprising finding is the lack of difference in predicition and delay intervals between manual and BCI control. This finding should be confirmed with more deliberate experiments to reduce the estimate uncertainty, as well as experiments of longer duration to establish whether the brain adjusts these intervals with learning. If true, this is a remarkable

and clear instance where the brain *cannot* adapt to optimally control a novel interface. This, and any similar findings should drive the areas in which a BCI decoding algorithm co-adapts to the brain to improve closed-loop performance where the brain cannot.

BIBLIOGRAPHY

[1] Johnny Accot and Shumin Zhai. More than dotting the i's — foundations for crossing-based interfaces. *Proceedings of the SIGCHI conference on Human factors in computing systems Changing our world, changing ourselves - CHI '02*, (1):73, 2002.

[2] Ravi Balasubramanian, Robert D Howe, and Yoky Matsuoka. Task performance is prioritized over energy reduction. *IEEE transactions on bio-medical engineering*, 56(5):1310–7, May 2009.

[3] Jose M. Carmena and Karunesh Ganguly. Emergence of a Stable Cortical Map for Neuroprosthetic Control. *PLoS Biology*, 7(7):e1000153, 2009.

[4] Jose M. Carmena, Mikhail A Lebedev, Roy E Crist, Joseph E O'Doherty, David M Santucci, Dragan F Dimitrov, Parag G Patil, Craig S. Henriquez, and Miguel A L Nicolelis. Learning to control a brain-machine interface for reaching and grasping by primates. *PLoS Biology*, 1(2):E42, November 2003.

[5] Géry Casiez and Nicolas Roussel. No more bricolage!: methods and tools to characterize, replicate and compare pointing transfer functions. *Proceedings of the 24th annual ACM symposium ...*, 2011.

[6] Géry Casiez and Daniel Vogel. The effect of spring stiffness and control gain with an elastic rate control pointing device. *Proceeding of the twenty-sixth annual CHI conference on Human factors in computing systems - CHI '08*, page 1709, 2008.

[7] Géry Casiez, Daniel Vogel, Ravin Balakrishnan, and Andy Cockburn. The Impact of Control-Display Gain on User Performance in Pointing Tasks. *Human-Computer Interaction*, 23(3):215–250, July 2008.

[8] Ozkan Celik, Dane Powell, and MK O'Malley. Impact of visual error augmentation

methods on task performance and motor adaptation. *Rehabilitation Robotics, 2009. ...*, pages 793–798, 2009.

[9] Steven M. Chase, Robert E Kass, and Andrew B Schwartz. Behavioral and neural correlates of visuomotor adaptation observed through a brain-computer interface in primary motor cortex. *Journal of neurophysiology*, 108(2):624–44, July 2012.

[10] Jennifer L Collinger, Brian Wodlinger, John E Downey, Wei Wang, Elizabeth C Tyler-Kabara, Douglas J Weber, Angus Jc McMorland, Meel Velliste, Michael L Boninger, and Andrew B Schwartz. High-performance neuroprosthetic control by an individual with tetraplegia. *The Lancet*, 6736(12):1–8, December 2012.

[11] John P. Cunningham, Vikash Gilja, Stephen I Ryu, and Krishna V. Shenoy. Methods for estimating neural firing rates, and their application to brain-machine interfaces. *Neural Networks: The Official Journal of the International Neural Network Society*, 22(9):1235–46, November 2009.

[12] J. C. F. De Winter and S. DE Groot. The effects of control-display gain on performance of race car drivers in an isometric braking task. *Journal of sports sciences*, 30(16):1747–1756, 2012.

[13] Julie Dethier, Paul Nuyujukian, Stephen I Ryu, Krishna V. Shenoy, and Kwabena Boahen. Design and validation of a real-time spiking-neural-network decoder for brain-machine interfaces. *Journal of neural engineering*, 10(3):036008, June 2013.

[14] Norman R. Draper and Harry Smith. *Applied Regression Analysis, 3rd Edition*. 1998.

[15] R. D. Ellis, a. Cao, a. Pandya, a. Composto, M. D. Klein, and G. Auner. Minimizing Movement Time in Surgical Telerobotic Tasks. *Proceedings of the Human Factors and Ergonomics Society Annual Meeting*, 49(11):1099–1103, September 2005.

[16] Joline M Fan, Paul Nuyujukian, Jonathan C Kao, Cynthia a Chestek, Stephen I Ryu, and Krishna V Shenoy. Intention estimation in brainmachine interfaces. *Journal of Neural Engineering*, 11(1):016004, February 2014.

[17] A. A. Fel'dbaum. Dual Control Theory, Parts I and II. *Automation and Remote Control*, 21(9,11):874–880, 1033–1039, 1960.

[18] E a Felton, R G Radwin, J a Wilson, and J C Williams. Evaluation of a modified Fitts law brain-computer interface target acquisition task in able and motor disabled individuals. *Journal of neural engineering*, 6(5):056002, October 2009.

[19] Eberhard E. Fetz. Operant Conditioning of Cortical Unit Activity. *Science*, 163(3870):955–958, 1969.

[20] Eberhard E. Fetz and MA Baker. Operantly conditioned patterns on precentral unit activity and correlated responses in .... *Journal of neurophysiology*, 1973.

[21] Jessica Fisher and Michael J Black. Motor cortical decoding using an autoregressive moving average model. *Proceedings of the International Conference of the IEEE Engineering in Medicine and Biology Society*, 2:2130–3, January 2005.

[22] Paul M Fitts. The information capacity of the human motor system in controlling the amplitude of movement. *Journal of Experimental Psychology*, 47(6):381–391, September 1954.

[23] George W Fraser, Steven M. Chase, Andrew Whitford, and Andrew B Schwartz. Control of a brain-computer interface without spike sorting. *Journal of neural engineering*, 6(5):055004, October 2009.

[24] Gregory J Gage, Kip a Ludwig, Kevin J Otto, Edward L Ionides, and Daryl R Kipke. Naive coadaptive cortical control. *Journal of Neural Engineering*, 2(2):52–63, June 2005.

[25] Gregory J Gage, K J Otto, K a Ludwig, and D R Kipke. Co-adaptive Kalman filtering in a naïve rat cortical control task. *Proceedings of the International Conference of the IEEE Engineering in Medicine and Biology Society*, 6:4367–70, January 2004.

[26] Apostolos P Georgopoulos, Andrew B Schwartz, and RE Kettner. Neuronal population coding of movement direction. *Science*, 233(4771):1416–1419, September 1986.

[27] Vikash Gilja, Paul Nuyujukian, Cynthia a Chestek, John P. Cunningham, Byron M Yu, Joline M Fan, Mark M. Churchland, Matthew T Kaufman, Jonathan C Kao, Stephen I Ryu, and Krishna V. Shenoy. A high-performance neural prosthesis enabled by control algorithm design. *Nature Neuroscience*, 15(November):1752–1757, November 2012.

[28] M Golub, Steven M. Chase, and MY Byron. Learning an internal dynamics model from control demonstration. *Proceedings of the 30th International Conference on Machine Learning*, 28, 2013.

[29] Matthew D Golub, BM Yu, and Steven M. Chase. Internal models engaged by brain-computer interface control. *Engineering in Medicine and ...*, pages 1327–1330, 2012.

[30] Suraj Gowda. Parameter estimation for maximizing controllability of linear brain-machine interfaces. *Engineering in Medicine ...*, pages 1314–1317, 2012.

[31] E Graham. Pointing on a computer display, 1996.

[32] Leigh R. Hochberg, Daniel Bacher, Beata Jarosiewicz, Nicolas Y. Masse, John D. Simeral, Joern Vogel, Sami Haddadin, Jie Liu, Sydney S. Cash, Patrick van der Smagt, and John P. Donoghue. Reach and grasp by people with tetraplegia using a neurally controlled robotic arm. *Nature*, 485(7398):372–375, May 2012.

[33] EJ Eun Jung Hwang, PM Paul M Bailey, and Richard A. Andersen. Volitional Control of Neural Activity Relies on the Natural Motor Repertoire. *Current Biology*, 23(5):353–361, March 2013.

[34] ISO. Ergonomic requirements for office work with visual display terminals (VDTs)Part 9Requirements for non-keyboard input devices (ISO 9241-9), 2002.

[35] R.E. Kalman. A new approach to linear filtering and prediction problems. *Journal of Basic Engineering*, 82(1):35–45, 1960.

[36] Preeya Khanna, Kelvin So, and Jose M. Carmena. Volitional phase control of neural oscillations using a brain-machine interface. *Neural Engineering (NER), ...*, pages 6–8, 2013.

[37] Sung-Phil Kim, John D. Simeral, Leigh R. Hochberg, John P. Donoghue, and Michael J Black. Neural control of computer cursor velocity by decoding motor cortical spiking activity in humans with tetraplegia. *Journal of neural engineering*, 5(4):455–476, December 2008.

[38] DA Kistemaker. The central nervous system does not minimize energy cost in arm movements. *Journal of . . .*, pages 2985–2994, 2010.

[39] Zheng Li, Joseph E. O'Doherty, Timothy L. Hanson, Mikhail A. Lebedev, Craig S. Henriquez, and Miguel A. L. Nicolelis. Unscented Kalman filter for brain-machine interfaces. *PloS One*, 4(7):e6243, July 2009.

[40] I. Scott MacKenzie. Fitts' law as a research and design tool in human-computer interaction. *HumanComputer Interaction*, 7(1):91–139, 1992.

[41] I. Scott MacKenzie, T. Kauppinen, and M. Silfverberg. Accuracy measures for evaluating computer pointing devices. In *Proceedings of the SIGCHI conference on Human factors in computing systems*, pages 9–16. ACM, 2001.

[42] Charlie Matlack, Chet Moritz, and Howard Chizeck. Applying best practices from digital control systems to BMI implementation. *Conference proceedings : ... Annual International Conference of the IEEE Engineering in Medicine and Biology Society. IEEE Engineering in Medicine and Biology Society. Conference*, 2012:1699–702, January 2012.

[43] Chet T Moritz and Eberhard E. Fetz. Volitional control of single cortical neurons in a brain-machine interface. *Journal of Neural Engineering*, 8(2):025017, April 2011.

[44] Norman S. Nise. *Control Systems Engineering.* Wiley, 6th edition, 2010.

[45] J.E. O'Doherty, M.A. Lebedev, T.L. Hanson, N.A. Fitzsimmons, and M.A.L. Nicolelis. A brain-machine interface instructed by direct intracortical microstimulation. *Frontiers in Integrative Neuroscience*, 3(September):1–10, 2009.

[46] Amy L Orsborn, Siddharth Dangi, Helene G Moorman, and Jose M. Carmena. Exploring time-scales of closed-loop decoder adaptation in brain-machine interfaces. *Conference proceedings : ... Annual International Conference of the IEEE Engineering in Medicine and Biology Society. IEEE Engineering in Medicine and Biology Society. Conference*, 2011:5436–9, January 2011.

[47] Amy L Orsborn, Siddharth Dangi, Helene G Moorman, and Jose M. Carmena. Closed-loop decoder adaptation on intermediate time-scales facilitates rapid BMI performance improvements independent of decoder initialization conditions. *IEEE transactions on neural systems and rehabilitation engineering : a publication of the IEEE Engineering in Medicine and Biology Society*, 20(4):468–77, July 2012.

[48] Liam Paninski, Matthew R Fellows, Nicholas G Hatsopoulos, and John P. Donoghue. Spatiotemporal tuning of motor cortical neurons for hand position and velocity. *Journal of Neurophysiology*, 91(1):515–32, 2004.

[49] Jangwoo Park, Hyunkyu Kim, Woojin Chung, and Shinsuk Park. Comparison of myocontrol and force control based on fitts law model. *International Journal of Precision Engineering and Manufacturing*, 12(2):211–217, April 2011.

[50] Sagi Perel, Patrick T. Sadtler, Jason M. Godlove, Stephen I. Ryu, Wei Wang, Aaron P. Batista, and Steven M. Chase. Direction and speed tuning of motor-cortex multiunit activity and local field potentials during reaching movements. *2013 35th Annual International Conference of the IEEE Engineering in Medicine and Biology Society (EMBC)*, pages 299–302, July 2013.

[51] Sunil M Prasad, Sandip M Prasad, Hersh S Maniar, Celeste Chu, Richard B Schuessler, and Ralph J Damiano. Surgical robotics: impact of motion scaling on task performance. *Journal of the American College of Surgeons*, 199(6):863–8, December 2004.

[52] Gopal Santhanam, Stephen I Ryu, Byron M Yu, Afsheen Afshar, and Krishna V. Shenoy. A high-performance brain-computer interface. *Nature*, 442(7099):195–8, July 2006.

[53] Hideaki Shimazaki and Shigeru Shinomoto. Kernel bandwidth optimization in spike rate estimation. *Journal of Computational Neuroscience*, 29 (1-2)(2010):171–182, August 2009.

[54] Garth Shoemaker, Takayuki Tsukitani, Yoshifumi Kitamura, and Kellogg S. Booth. Two-Part Models Capture the Impact of Gain on Pointing Performance. *ACM Transactions on Computer-Human Interaction*, 19(4):1–34, December 2012.

[55] John D. Simeral, S-P Kim, Michael J Black, John P. Donoghue, and Leigh R. Hochberg. Neural control of cursor trajectory and click by a human with tetraplegia 1000 days after implant of an intracortical microelectrode array. *Journal of neural engineering*, 8(2):025027, April 2011.

[56] Marc W Slutzky, Luke R Jordan, Eric W Lindberg, Kevin E Lindsay, and Lee E Miller. Decoding the rat forelimb movement direction from epidural and intracortical field potentials. *Journal of neural engineering*, 8(3):036013, June 2011.

[57] Jacob J Sosnoff and Karl M Newell. Information processing limitations with aging in the visual scaling of isometric force. *Experimental brain research. Experimentelle Hirnforschung. Expérimentation cérébrale*, 170(3):423–32, April 2006.

[58] R. William Soukoreff and I. Scott MacKenzie. Towards a standard for pointing device evaluation, perspectives on 27 years of Fitts law research in HCI. *International Journal of Human-Computer Studies*, 61(6):751–789, December 2004.

[59] R. William Soukoreff, Jian Zhao, and Xiangshi Ren. The Entropy of a Rapid Aimed Movement: Fitts Index of Difficulty versus Shannons Entropy. *Human-Computer InteractionINTERACT . . .*, pages 222–239, 2011.

[60] Eran Stark and Moshe Abeles. Predicting movement from multiunit activity. *The Journal of Neuroscience*, 27(31):8387–94, August 2007.

[61] Aaron J Suminski, Dennis C Tkach, Andrew H Fagg, and Nicholas G Hatsopoulos. Incorporating feedback from multiple sensory modalities enhances brain-machine in-

terface control. *The Journal of neuroscience : the official journal of the Society for Neuroscience*, 30(50):16777–87, December 2010.

[62] Dawn M Taylor, Stephen I Helms Tillery, and Andrew B Schwartz. Direct cortical control of 3D neuroprosthetic devices. *Science (New York, N.Y.)*, 296(5574):1829–32, June 2002.

[63] Dawn M Taylor, Stephen I Helms Tillery, and Andrew B Schwartz. Information conveyed through brain-control: cursor versus robot. *IEEE transactions on neural systems and rehabilitation engineering : a publication of the IEEE Engineering in Medicine and Biology Society*, 11(2):195–9, July 2003.

[64] E Tse and M Athans. Adaptive stochastic control for a class of linear systems. *Automatic Control, IEEE Transactions on*, (1), 1972.

[65] E Tse, Y Bar-Shalom, and L Meier III. Wide-sense adaptive dual control for nonlinear stochastic systems. *Automatic Control, IEEE ...*, 18(2):98–108, 1973.

[66] Meel Velliste, S Perel, Andrew S Whitford, MC Spalding, and Andrew B Schwartz. Cortical control of a prosthetic arm for self-feeding. *Nature*, 453, 2008.

[67] Alan Traviss Welford. *Fundamentals of Skill*. Methuen, London, 1971.

[68] Johan Wessberg and Miguel a L Nicolelis. Optimizing a linear algorithm for real-time robotic control using chronic cortical ensemble recordings in monkeys. *Journal of Cognitive Neuroscience*, 16(6):1022–35, 2004.

[69] Johan Wessberg, C R Stambaugh, J D Kralik, P D Beck, M Laubach, J K Chapin, J Kim, S J Biggs, M a Srinivasan, and M a Nicolelis. Real-time prediction of hand trajectory by ensembles of cortical neurons in primates. *Nature*, 408(6810):361–5, November 2000.

[70] Francis R Willett, Aaron J Suminski, Andrew H Fagg, and Nicholas G Hatsopoulos. Improving brain-machine interface performance by decoding intended future movements. *Journal of neural engineering*, 10(2):026011, April 2013.

[71] Jacob O. Wobbrock and Kristen Shinohara. The effects of task dimensionality, endpoint deviation, throughput calculation, and experiment design on pointing measures and models. In *Proceedings of the ACM Conference on Human Factors in Computing Systems (CHI '11)*, pages 1639–1648, Vancouver, British Columbia, 2011. New York: ACM Press.

[72] Byron M Yu, Caleb Kemere, Gopal Santhanam, Afsheen Afshar, Stephen I Ryu, Teresa H Meng, Maneesh Sahani, and Krishna V. Shenoy. Mixture of trajectory models for neural decoding of goal-directed movements. *Journal of neurophysiology*, 97(5):3763–80, May 2007.

[73] Xuan Zhang and I. Scott MacKenzie. Evaluating Eye Tracking with ISO 9241 - Part 9. pages 779–788, 2007.

VITA

Charlie grew up outside of San Digeo, CA, before attending Harvey Mudd College in Claremont, CA. After earning a Bachelor of Science degree in engineering in 2004, he began graduate school at the University of Washington.